Tactile Aerial Grasping via High-Resolution Touch on Drones

Thesis Report

Muhammad Arham Elahi

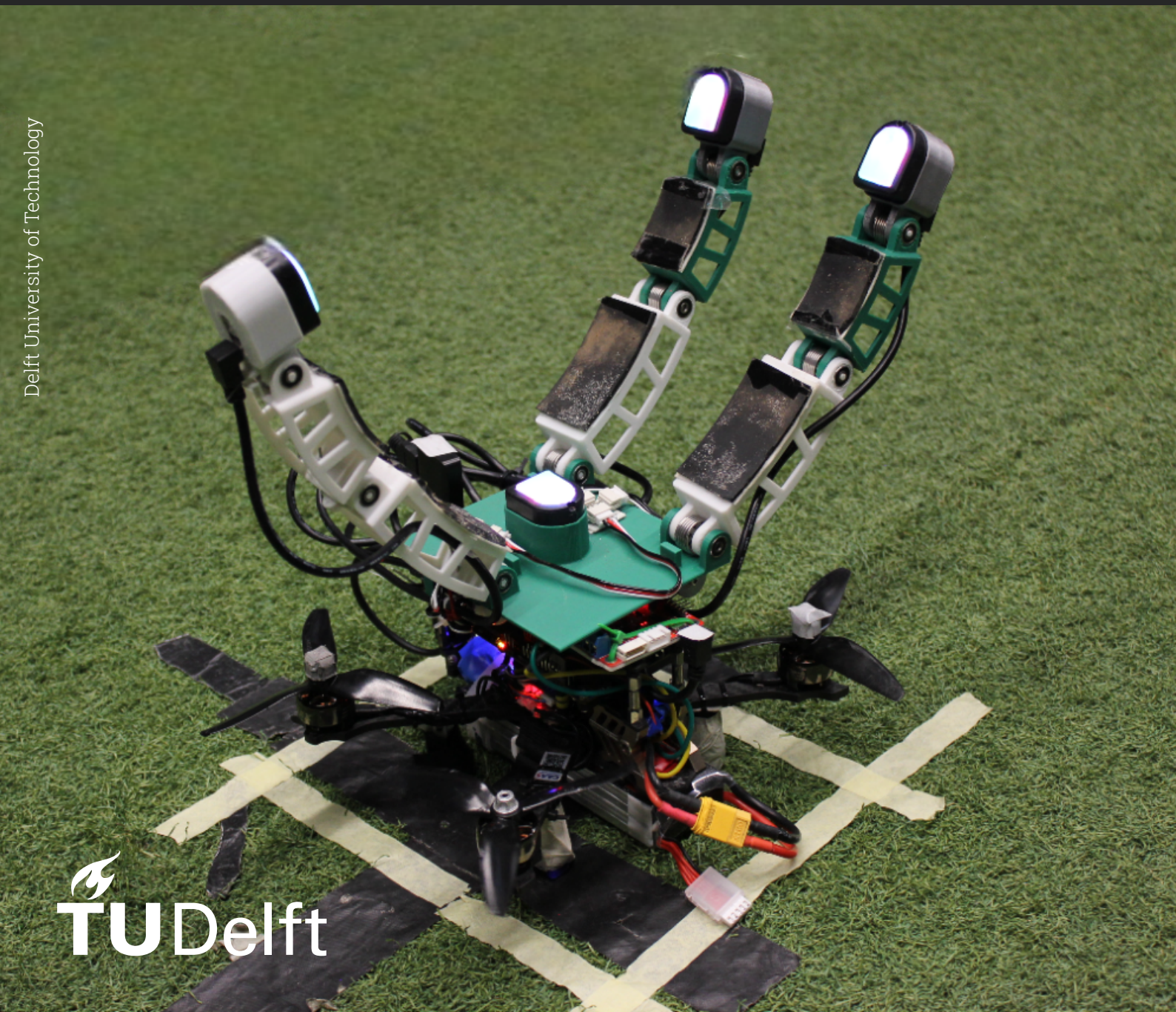

Delft University of Technology

TU Delft

Tactile Aerial Grasping via High-Resolution Touch on Drones

Thesis Report

by

Muhammad Arham Elahi

Thesis Committee:

Chair:	Dr. Ewoud Smeur
Supervisor:	Dr. Salua Hamaza
External Member:	Dr. Alessandro Bombelli
Coach:	Anton Bredenbeck
Coach:	Martijn Brummelhuis
Project Duration:	November, 2024 - August, 2025
Student Number:	5213320
Faculty:	Faculty of Aerospace Engineering, Delft

TU Delft

Preface

This thesis marks the culmination of my studies in Aerospace Engineering and the conclusion of my time in Delft. It has been an incredible journey since I first arrived in the Netherlands as a 17-year-old in 2020, leading up to my graduation in 2025. This work focuses on the design, development, and testing of a perching drone equipped with high-resolution tactile sensing, aiming to improve robustness and adaptability in aerial manipulation tasks.

The past nine months devoted to this project have been both challenging and rewarding. They have given me the opportunity to tackle real engineering challenges and work with hardware that was entirely unfamiliar to me at the start. This process has allowed me to develop valuable knowledge in drone design, ROS programming, and command-line interfacing. The research combined theoretical calculations with extensive design iteration and hands-on testing, an approach that often presented significant challenges but also taught me resilience and strengthened my mental fortitude.

I would like to express my sincere gratitude to my thesis supervisor, Dr. Salua Hamaza, for her guidance throughout the project. My appreciation also goes to my coaches, Anton Bredenbeck and Martijn Brummelhuis, for always being available and for providing valuable insights and encouragement. I am thankful to my colleagues and friends at the MAVLAB, particularly Luc Thomas, Michael van Breukelen, Georg Strunk, and Justin Dubois, for creating a fun and collaborative environment and for keeping me company during the rollercoaster that was the thesis.

Finally, I am deeply grateful to my parents, Muhammad Ather Elahi and Sabahat Ather, for their unwavering support and encouragement. My siblings, Muhammad Raiyan Elahi and Alishba Ather, have always been there to take my mind off things when needed. Lastly, I would like to thank my friends, particularly Ana Maria Mekereshvili, Bartosz Jemiol, Affan Siddiqui, Thomas Muller, Dominik Spoljaric, Luka Distelbrink, Caitlin Clark, Sahir Sujahudeen, and Mila Dobrovinskaya, for always checking in on me, making sure I was doing well, and reminding me to have lunch. Their belief in me has been a constant source of motivation.

Muhammad Arham Elahi
Delft, August 2025

Contents

1

Introduction

Over the past decade, drones have progressed from simple data-gathering platforms into systems capable of directly interacting with their surroundings. This shift has opened opportunities in areas such as infrastructure inspection, environmental monitoring, and precision agriculture, where the ability to physically manipulate or attach to objects greatly expands operational scope. Among these emerging capabilities, perching, the act of securing a drone to a surface, stands out as a particularly valuable skill. By perching, a drone can conserve energy, maintain a stable observation platform, and extend its mission duration well beyond the limits of continuous flight.

Despite these advantages, perching remains technically challenging. Aerial platforms must approach and interact with a target without the benefit of ground reaction forces, making stability and force control inherently more complex. Achieving a reliable perch requires precise alignment, the regulation of contact forces, and adaptability to target surfaces that may be uncertain in position, shape, or orientation. Traditionally, vision systems have been used to locate and approach perching targets, but they struggle in close-range scenarios where occlusions occur, lighting conditions vary, or the target is partially hidden by the manipulator itself. As a result, reliance on vision alone often limits the robustness of perching maneuvers. Tactile sensing offers a complementary pathway by directly measuring the physical interaction between the drone and its environment. These capabilities can enable the drone to make corrective adjustments even when visual information is unavailable or unreliable.

This research addresses these limitations by integrating high-resolution optical tactile sensors into a perching drone. Since the sensors are designed for use as fingertips, grasping is selected as the preferred method of perching. The aim is to move beyond basic contact confirmation toward richer contact characterization, enabling the platform to detect both position and orientation errors in real time and correct them during the perching process. The central objective is to design, manufacture, and test a system capable of autonomous perching regardless of its initial approach alignment. The work focuses on four main goals: (1) designing a gripper that enables robust and secure perching, (2) integrating optical tactile sensors into the perching mechanism, (3) developing a control strategy that fuses tactile and positional feedback for alignment correction, and (4) evaluating the system's performance through both bench-top and in-flight experiments on targets of varying size and material. The overall research question is:

> **How can the integration of high-resolution tactile sensors enhance the functionality, adaptability, and robustness of an aerial grasping drone, enabling contact localisation, shape inference, and autonomous grasping via tactile-driven control?**

The remainder of this report is organized as follows. chapter 2 presents the research conducted to achieve the goals specified above. chapter 3 provides an extensive literature review on aerial manipulators, perching drones, and tactile sensing in robotics.

2

Scientific Article

Tactile Aerial Grasping via High-Resolution Touch on Drones

By Muhammad Arham Elahi

***Abstract*— This thesis presents the design, development, and experimental validation of a perching drone equipped with an underactuated robotic gripper and tactile sensing for grasping onto structures. Perching extends drone endurance for applications such as long-term monitoring, while tactile sensing enables precise alignment when visual data is unreliable. A control strategy combining position-based control with tactile feedback is implemented using DIGIT tactile sensors for contact-aware adjustments. Two per-pixel inference models convert RGB images into tactile information: a sensitive contact model for binary contact detection and a depth reconstruction model that estimates surface normals, which is then used to determine the contact surface orientation. After outlier filtering, the depth model achieves a mean absolute error of 5.32° in orientation estimation. Experiments demonstrate reliable grasping with up to 12 cm of position error and successful correction of both position and orientation using simulated tactile input. These results highlight the potential of tactile-based strategies for robust aerial manipulation in uncertain environments.**

I. INTRODUCTION

In recent years, aerial robotics has evolved from passive data collection platforms into systems capable of active physical interaction with their environment. Applications in domains such as precision agriculture, environmental monitoring, and infrastructure inspection increasingly demand drones that can not only observe but also interact with objects. Aerial manipulators, drones equipped with robotic appendages, have emerged to meet this challenge. However, achieving reliable physical interaction, such as grasping or perching, remains significantly more complex than passive flight due to the absence of ground reaction forces and the need for precise control of forces and torques.

Among interaction capabilities, perching, the ability of a drone to securely attach to its environment, is of particular interest. Perching enables aerial robots to conserve energy, extend mission durations, and perform stable long-term operations such as inspection, monitoring, or surveillance. Despite its promise, perching presents several technical challenges, including maintaining stability during contact, regulating grasping forces, and adapting to uncertain or dynamic environments. These challenges are compounded by the limitations of conventional computer vision, particularly at close range. In such situations, it is prone to occlusions, affected by poor lighting conditions, and unable to detect contact forces.

To address these limitations, tactile sensing is identified as a critical component of more robust aerial manipulation. Tactile sensors can detect small details of contact interactions, such as force distribution, slip, and surface geometry, offering complementary capabilities to vision, which can provide global target position estimates from a distance.

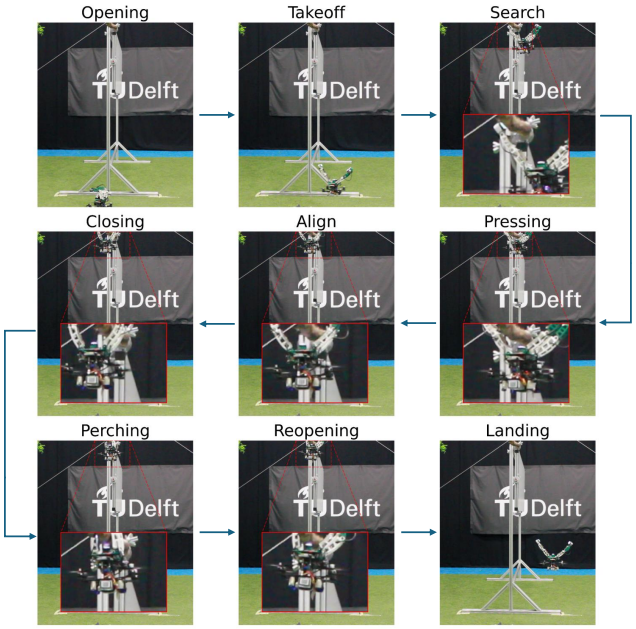

Fig. 1: Autonomous Perching Overview: The drone initializes by opening its fingers and activating the sensors. It then takes off and searches for the bar. Upon contact, it adjusts its position so the base is directly below the branch. Next, it presses to obtain an orientation estimate and yaws to align with the branch before closing its fingers to perch. Finally, it reopens its fingers and lands.

However, while tactile sensing has seen widespread adoption in ground-based and industrial robotics, its integration into aerial systems remains rare [1–3]. Early aerial manipulation studies that used force sensing, such as contour-following tasks, showed the potential of touch feedback [4, 5]. However, fully utilizing high-resolution tactile information for aerial perching is still largely unexplored.

Previous perching drones have relied primarily on vision for contact detection. Even those incorporating tactile sensing often use binary touch sensors for basic contact confirmation. While this enables simple grasp detection, it requires the drone to approach the perching surface in a predefined orientation [6]. Capacitive tactile sensors add a further limitation, as they are sensitive only to conductive materials, significantly reducing their adaptability.

To overcome these limitations, this research aims to design, manufacture, and test a novel perching drone equipped with high-resolution optical tactile sensors, specifically, DIGIT sensors, at key contact points. By using tactile feed-

back not merely for binary contact confirmation but for richer contact characterization, the drone can perform autonomous perching maneuvers as shown in Figure 1.

This work evaluates the performance improvements enabled by high-resolution tactile feedback in aerial perching tasks. Experimental validation involves bench tests of tactile data quality and in-flight perching trials on cylindrical structures of varying radii and material. Through these experiments, the research seeks to answer the central question:

> **How can the integration of high-resolution tactile sensors enhance the functionality, adaptability, and robustness of an aerial grasping drone, enabling contact localisation, shape inference, and autonomous grasping via tactile-driven control?**

The remainder of this paper is structured as follows: section II reviews related work on aerial manipulation, perching strategies, and tactile sensing technologies. section III gives an outlook on the mechanical design process and aerial platform assembly. section IV presents the methodology, including sensor modeling and control strategies. section V discusses the experimental results obtained, and section VI offers conclusions and directions for future research.

II. Related Work

The development of aerial manipulators and perching drones is gaining increasing attention as drones evolve from passive sensors to active agents capable of interacting with their environment. This section discusses relevant advances in aerial perching mechanisms in subsection II-A, the integration of tactile sensing into aerial systems in subsection II-B, and the design and use of high-resolution optical tactile sensors, with particular emphasis on the DIGIT sensor in subsection II-C.

A. Perching Drone Design

Research on perching drones can be broadly categorized into three main biologically inspired approaches: grasping (bird-like claws) [7], attaching (gecko-inspired adhesives) [8], and embedding (insect-inspired spines) [9].

Notable grasping-based designs include the avian-inspired perching drone with underactuated claws that passively transform impact energy into grasp force [10], and the OpenHand gripper from Yale, which uses compliant, underactuated fingers for robust grasping despite lacking tactile sensing [11]. Unique mechanisms such as the SpiderMAV, which perches using gas-launched anchors [12], and soft tendril-inspired grippers [13] also demonstrate the diversity of approaches.

However, most existing perching systems rely on ground truth or vision to obtain the target pose. This information is not always available with sufficient accuracy, especially when the drone is close to the target object. Tactile information from the environment can maintain closed-loop feedback, significantly increasing adaptability.

B. Tactile Sensing in Robotics and Aerial Systems

Tactile sensing is a critical component in ground-based robotic manipulation. It provides real-time information on contact forces, object geometry, and texture, enabling robust grasping and reactive control [14]. Technologies for tactile sensing include resistive, capacitive, piezoelectric, and optical sensors, each with trade-offs in terms of resolution, sensitivity, stretchability, and environmental robustness.

Capacitive tactile sensors, for example, have been used in robotic hands and perching drones to detect simple contact events [6]. However, these sensors often exhibit nonlinear responses, require careful calibration, and provide limited spatial information. Their susceptibility to electromagnetic interference and environmental noise further reduces the reliability in dynamic environments [14].

In aerial systems, tactile sensing is still emerging. Some recent studies have explored using force sensors to enable tasks like contour following and compliant inspection [4, 15]. However, high-resolution tactile sensors remain largely absent in drone platforms, due to constraints on payload, power, data processing and other practical limitations.

C. Optical Tactile Sensors

Optical tactile sensors represent a promising direction for aerial applications due to their high resolution, immunity to electromagnetic interference, and ability to capture rich contact geometry. These sensors operate by monitoring changes in light caused by surface deformation. Variants include fiber-optic, internal reflection, and camera-based systems [16].

The DIGIT sensor, introduced by Lambeta et al. [17], is a compact, low-cost optical tactile sensor that captures high-resolution images of contact deformations using a camera and multicolor LEDs. Its exploded view is shown in Figure 2. It is particularly well-suited for integration into robot end-effectors and grippers, offering sub-millimeter detail at a theoretical maximum of 60 frames per second. Depending on the sensing task, the elastomer layer in DIGIT can be customized for reflectivity or even include embedded features.

The sensor has been successfully used for tasks like slip detection, object manipulation, and tactile servo control on ground robots [17, 18]. A derivative known as **DigiTac** combines the DIGIT's base (illumination and camera) with the TacTip's soft, curved skin to enhance compliance and surface tracking [18]. However, stiffness-induced contact biasing and durability challenges such as skin tearing have been reported during extended use.

III. Mechanical Design

Since the DIGIT tactile sensors are designed for use as fingertips, the grasping method is chosen for perching. The drone is designed with the dual objective of enabling secure interaction with the environment while maintaining a lightweight construction suitable for aerial deployment. The goal is to build an underactuated, compliant, three-fingered grasping mechanism.

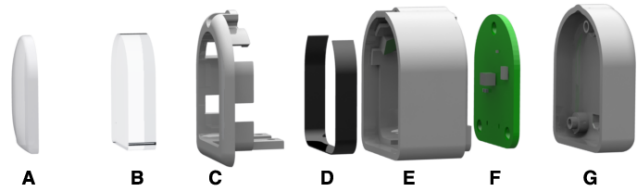

Fig. 2: Exploded view of a DIGIT sensor. A) elastomer, B) acrylic window, C) snap-fit holder, D) lighting PCB, E) plastic housing, F) camera PCB, G) back housing [17].

A. Gripper Design

The grasping mechanism consists of a three-fingered, underactuated gripper, with each finger comprising three phalanges connected via revolute joints and tensioned by torsional springs. The faces of the middle and base phalanges are covered with rubber pads, which increase friction and also serve as a soft, compliant contact surface. This arrangement ensures inherent compliance, allowing the fingers to passively adapt to irregular geometries without requiring high-precision control. The design reduces the number of required actuators, lowering both the system's weight and computational load, while maintaining grasp adaptability. It facilitates secure grasping of cylindrical objects such as pipes, rods, or branches.

The design goal is to passively conform to cylindrical perching surfaces of various radii while generating sufficient grasp force to support the drone's weight during perching. A quasi-static force analysis using geometric and mechanical constraints is used to determine the spring stiffnesses and phalange lengths.

A static equilibrium model is developed to understand load distribution across the finger joints, where the following assumptions are made:

- Each finger supports exactly one-third of the drone's total weight W, acting vertically.
- Each finger consists of three straight phalanges, each making tangential contact with the cylindrical surface.
- The normal and tangential contact forces on each phalange act at the phalange's midpoint.
- The friction coefficient between the finger and cylinder is set to $\mu = 0.5$, based on a conservative estimate of the friction between the rubber surface of the finger and other materials [19].
- The horizontal clamping force that may be present due to the presence of multiple fingers is neglected.

As shown in Figure 3, let the three phalanges be of lengths L_1, L_2, L_3, and contact angles with the cylinder be $\theta_1, \theta_2, \theta_3$, respectively. The phalange lengths are chosen as:

$$L_1 = 50\,\text{mm}, \quad L_2 = 70\,\text{mm}, \quad L_3 = 95\,\text{mm}$$

Each phalange experiences a normal force $F_{i,n}$ and tangential force $F_{i,t}$, for $i = 1, 2, 3$. With these assumptions, the system can be described by the following equilibrium equations:

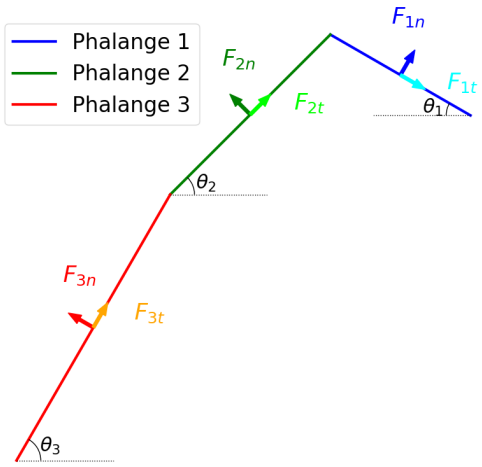

Fig. 3: Schematic of the Finger Representation used for the quasi-static analysis showcasing the angles (θ_i), the normal forces ($F_{i,n}$) and tangential forces ($F_{i,t}$) for all three phalanges.

1) **Horizontal Force Balance:**

$$\begin{aligned} &F_{1t}\cos(\theta_1) + F_{2t}\cos(\theta_2) + F_{3t}\cos(\theta_3) \\ &+ F_{1n}\sin(\theta_1) - F_{2n}\sin(\theta_2) - F_{3n}\sin(\theta_3) = 0 \end{aligned} \quad (1)$$

2) **Vertical Force Balance:**

$$\begin{aligned} &F_{1n}\cos(\theta_1) + F_{2n}\cos(\theta_2) + F_{3n}\cos(\theta_3) \\ &- F_{1t}\sin(\theta_1) + F_{2t}\sin(\theta_2) + F_{3t}\sin(\theta_3) = \frac{W}{3} \end{aligned} \quad (2)$$

3) **Moment Balance at the base:**

$$\begin{aligned} &F_{1n}\left(\tfrac{L_1}{2} + L_2\cos(\theta_1+\theta_2) + L_3\cos(\theta_1+\theta_3)\right) \\ &+ F_{2n}\left(\tfrac{L_2}{2} + L_3\cos(\theta_3-\theta_2)\right) + F_{3n}\left(\tfrac{L_3}{2}\right) \\ &+ F_{1t}\left(-L_2\cos(\theta_1+\theta_2) - L_3\sin(\theta_1+\theta_3)\right) \\ &+ F_{2t}\left(-L_3\sin(\theta_3-\theta_2)\right) = W\cdot b \end{aligned} \quad (3)$$

These three equations relate six unknowns: $F_{1n}, F_{2n}, F_{3n}, F_{1t}, F_{2t}, F_{3t}$. A numerical solver is implemented using the cost function shown in Equation 4 with $\alpha > 1$, which minimizes reliance on tangential (frictional) forces in favor of normal forces. The forces can then be used to calculate the joint torques and the required stiffness for springs with an initial angle of 270 degrees, as shown in Equation 5. This approach enables the estimation of valid solutions across a range of target radii. The results are presented in Figure 4 for $\alpha = 10$.

$$f(x) = \alpha\cdot(F_{1t} + F_{2t} + F_{3t}) + (F_{1n} + F_{2n} + F_{3n}) \quad (4)$$

$$\begin{bmatrix} T_1 \\ T_2 \\ T_3 \end{bmatrix} = \begin{bmatrix} L_1/2 & 0 & 0 \\ L_1/2 & L_2/2 & 0 \\ L_1/2 & L_2/2 & L_3/2 \end{bmatrix} \begin{bmatrix} F_{1n} \\ F_{2n} \\ F_{3n} \end{bmatrix} \quad (5)$$
$$\begin{bmatrix} k_1 \\ k_2 \\ k_3 \end{bmatrix} = \begin{bmatrix} T_1/(\frac{3\pi}{2} - \theta_1 - \theta_2) \\ T_2/(\frac{3\pi}{2} + \theta_2 - \theta_3) \\ T_3/(\pi + \theta_3) \end{bmatrix}$$

The results as shown in Figure 4 revealed that:

- For small radii ($< 40\,\mathrm{mm}$), the second phalange contributes most significantly to weight support (F_{2n} dominates) with the third phalange also contributing (F_{3n} assists).
- As the radius increases, the load progressively shifts to the first phalange, leading to an increase in F_{1n}.
- For even larger radii ($> 55\,\mathrm{mm}$), the required tangential force on the first phalange (F_{1t}) increases significantly. This occurs because F_{1n} alone can no longer generate a sufficient counterclockwise moment to balance the clockwise moments produced by the other normal forces, particularly F_{2n} and F_{2t}. As a result, F_{1t} must compensate to maintain equilibrium. However, the horizontal force introduced by F_{1t} must also be balanced, leading to a further increase in F_{2n}. Beyond approximately $60\,\mathrm{mm}$, these constraints make it impossible for the solver to find a valid solution.

These trends are illustrated even more clearly in Figure 5, which shows how force loading transitions across a range of radii.

These trends are used to guide spring selection. The first two joints (at the base and middle) experience higher torques due to the greater load-bearing requirement. The fingertip joint, experiencing lower moments, requires a weaker spring. In the absence of manufacturer data, spring constants are estimated using the standard torsional spring stiffness equation:

$$k = \frac{Ed^4}{10.8 D_o N} \quad (6)$$

where E is the elastic modulus, d is the wire diameter, D_o is the outer diameter of the spring, and N is the number of coils. This informed the use of the springs shown in Table I.

TABLE I: Properties of springs used in the finger joints.

Joint	d (mm)	D_o (mm)	N (-)	k (Nm/rad)
Base and Middle Joints	1.22	15.24	6.75	0.0695
Distal Joint	1.02	12.98	6.75	0.0398

Actuation of the fingers is provided by three Feetech STS3032 serial bus servomotors, one for each finger. These motors are mounted on the baseplate and connected to the finger digits via routed nylon tendon lines, enabling coordinated grasping motions through tendon tension.

The gripper is mounted in a top-down configuration, placing it above the drone's center of gravity. This design choice improves passive perching stability, minimizing the motor thrust required to maintain a perched state. It also eliminates interference with landing skids and enables perching onto elevated cylindrical structures, while preserving the drone's ability to land conventionally when required.

Each fingertip and the base of the gripper are equipped with a DIGIT sensor. The sensors are mechanically mounted using a press-fit clamp design.

B. Aerial Platform

The base platform is constructed around a modified SpeedyBee FS225 V2 5-inch quadcopter frame, with an additional platform added to host the flight computer and enable attachment of the gripper. Each arm of the frame houses a standard brushless motor for flight control, while a central compartment accommodates the flight electronics, battery, and gripper assembly.

The drone is equipped with a MatekSys H743-Slim V3 flight controller running PX4 Autopilot firmware [20]. An Orange Pi 5B is mounted onboard to run the Finite State Machine and perform tactile data processing, motor actuation, and flight path computation. An OptiTrack MOCAP system is utilized for pose estimation. Power is supplied by a 4S LiPo battery. The total weight of the aerial platform is 1.2 kg, including the battery. The drone is shown in open and closed positions in Figure 6.

IV. Methodology

This section outlines the approach used to enable tactile-based perching. It covers both the processing pipeline for tactile data and the development of the control strategy.

A. Tactile Data Processing Pipeline

The tactile data acquired from the DIGIT sensors is processed using supervised learning models trained to extract two types of information: surface deformation (depth) and contact regions. Each model operates per pixel, enabling dense interpretation of the sensor's high-resolution image stream.

1) Model Structure: To reduce computational overhead and accommodate onboard inference on the Orange Pi 5B, the DIGIT sensors are configured to operate at their lowest supported settings: a frame rate of 30 Hz and a resolution of 320×240 pixels. The images are converted from RGB to HSV color space, as this allows for the separation of intensity and color information. Each input pixel is normalized and represented by a five-dimensional vector $\{x, y, h, s, v\}$, where (x, y) denotes the pixel coordinates and (h, s, v) are the color channels.

The neural network architecture used for depth and contact estimation consists of a fully connected feedforward network with three hidden layers, each containing 32 nodes and ReLU activation functions as shown in Figure 7. The networks are trained offline using a labeled dataset of tactile images with corresponding ground truth outputs, and then exported as PyTorch scripts for deployment. During flight, inference is executed live onboard the Orange Pi.

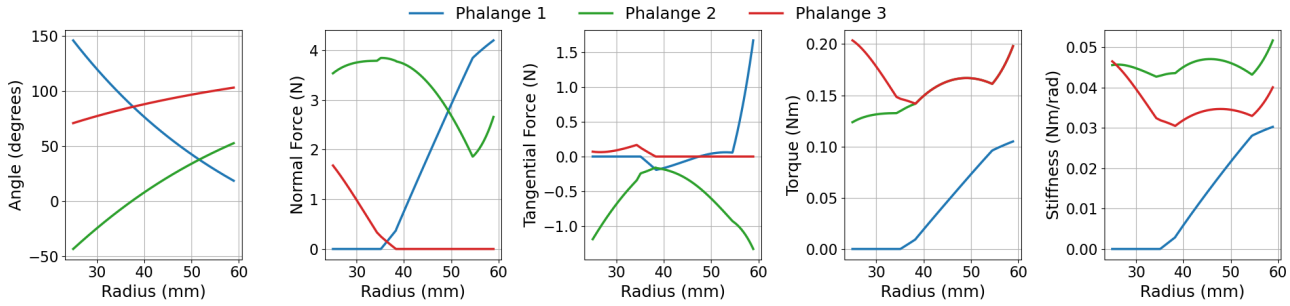

Fig. 4: Quasi-static analysis results. The far-left plot shows the angle of each phalange when wrapping around a cylinder, while the left plot shows the corresponding normal forces. The middle plot shows the tangential forces. These forces result in the joint torques in the right plot and the required spring stiffnesses in the far-right plot.

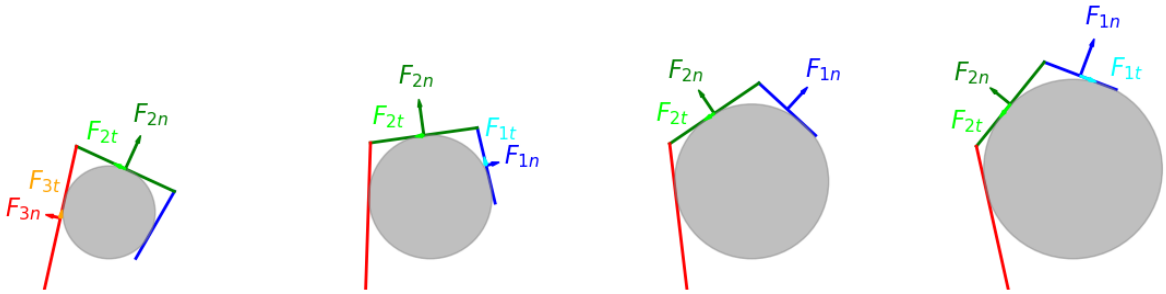

Fig. 5: Finger configurations for radii of 30, 40, 50, and 58 mm, showing a clear transition of load from the second phalange to the first phalange.

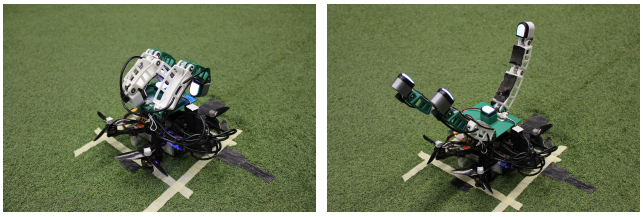

(a) Closed (b) Open

Fig. 6: The Drone shown in the closed (left) and open (right) positions.

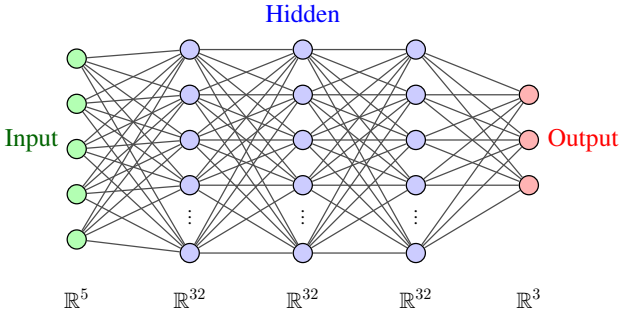

Fig. 7: Neural network architecture for the depth model with 5 input nodes (x, y, h, s, v), three hidden layers with 32 nodes each, and 3 output nodes (n_x, n_y, n_z). The contact model shares the same architecture, except it has a single output node (C).

2) Ground Truth Generator: The ground truth generator produces per-pixel normal vectors and contact masks for analytically defined shapes. Each training image is paired with a normal map that describes the surface normal at every valid pixel (x, y) as a unit vector, mapped from $[-1, 1]$ to $[0, 1]$ for consistency.

For a **sphere**, the normal vector is defined by an inclination angle θ_{xz} and an azimuth angle θ_{xy}, as given in Equation 7.

$$\mathbf{n} = \begin{bmatrix} \cos(\theta_{xz})\cos(\theta_{xy}) \\ \cos(\theta_{xz})\sin(\theta_{xy}) \\ \sin(\theta_{xz}) \end{bmatrix}. \tag{7}$$

The angles are computed from the sphere's known center (x_c, y_c) and radius r_{sphere} using Equation 8.

$$\begin{aligned} d &= \sqrt{(x - x_c)^2 + (y - y_c)^2} \\ \theta_{xz} &= \arccos\left(\frac{d}{r_{\text{sphere}}}\right) \\ \theta_{xy} &= \arctan\left(\frac{y - y_c}{x - x_c}\right) \end{aligned} \tag{8}$$

Pixels are included only if $d \leq r_{\text{sphere}}$. The resulting normal is then normalized and shifted to the range $[0, 1]$.

For a **cylinder**, the elliptical contact patch is modeled as a series of semicircular cross-sections distributed along the semi-major axis, producing a symmetric dome-like deformation. Each pixel (x, y) is first mapped to normalized ellipse

coordinates (x_e, y_e) by projecting its displacement vector $\mathbf{d}$ onto the semi-major and semi-minor axes as shown in Equation 9.

$$\begin{aligned} \mathbf{d} &= \begin{bmatrix} x - c_x \\ y - c_y \end{bmatrix} \\ x_e = p_{\text{major}} &= \frac{\mathbf{d} \cdot \hat{\mathbf{a}}_{\text{major}}}{r_{\text{l}}} \\ y_e = p_{\text{minor}} &= \frac{\mathbf{d} \cdot \hat{\mathbf{a}}_{\text{minor}}}{r_{\text{s}}} \end{aligned} \tag{9}$$

Here, (c_x, c_y) is the ellipse center, $\hat{\mathbf{a}}_{\text{major}}$ and $\hat{\mathbf{a}}_{\text{minor}}$ are unit vectors along the axes, and r_{l}, r_{s} are the respective radii. The normalized coordinates (x_e, y_e) must satisfy $x_e^2 + y_e^2 \leq 1$.

At each x_e, the local cross-section is modeled as a semi-circle with radius Equation 10.

$$y_c = y_e \cdot \frac{r_s}{r_{\text{cylinder}}}, \quad |y_c| \leq 1. \tag{10}$$

The local depth function and its derivative (the slope) are defined by Equation 11.

$$z(y_c) = \sqrt{1 - y_c^2}, \quad s = \frac{dz}{dy_c} = -\frac{y_c}{\sqrt{1 - y_c^2}}. \tag{11}$$

This slope defines the local surface inclination in the 2D cross-section. The local tangent angle satisfies $\tan(\theta) = s$, so the unit normal in the cross-sectional plane is given below:

$$\mathbf{n}_c = \begin{bmatrix} 0 \\ \sin(\theta) \\ \cos(\theta) \end{bmatrix} = \begin{bmatrix} 0 \\ \frac{s}{\sqrt{1+s^2}} \\ \frac{1}{\sqrt{1+s^2}}. \end{bmatrix} \tag{12}$$

To express this normal in the global image frame, the local slope component is rotated along the semi-minor axis, yielding Equation 13:

$$\begin{aligned} \begin{bmatrix} v_x \\ v_y \end{bmatrix} &= \sin(\theta)\, \hat{\mathbf{a}}_{\text{minor}} = \frac{s}{\sqrt{1+s^2}}\, \hat{\mathbf{a}}_{\text{minor}} \\ \mathbf{n} &= \begin{bmatrix} v_x \\ v_y \\ \cos(\theta) \end{bmatrix} \end{aligned} \tag{13}$$

Finally, the normal vector is normalized and shifted to $[0, 1]$. This ensures that the semi-major axis center line always produces a normal vector pointing directly outward $(0, 0, 1)$, while the local cross-sectional slope varies smoothly toward the elliptical boundary. This better approximates the contact deformation of a soft elastomer under load.

Examples of the generated ground truth data for both spherical and cylindrical deformations are shown in Figure 8. For the contact model, the ground truth marks the interior of the deformation as contact (value 1) and everything outside as non-contact (value 0). For the depth model, the background region of each image is assigned a default normal vector of $[0, 0, 1]$, which maps to $[127, 127, 255]$ in the RGB color space after normalization and rescaling. This corresponds to the bluish color visible in the non-contact regions of the figure. The spherical deformation demonstrates a red shift toward the right side as the n_x component increases, and a green shift downwards as the n_y component grows, reflecting the local surface orientation. The cylindrical deformation shows a symmetrical pattern across its centerline: the center points directly outward while the side regions' red value gradually shifts, with n_x increasing to the right, indicating the semicircular curvature around the cylinder's surface.

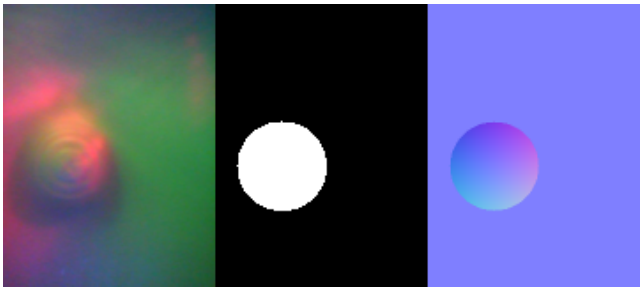

(a) Sphere

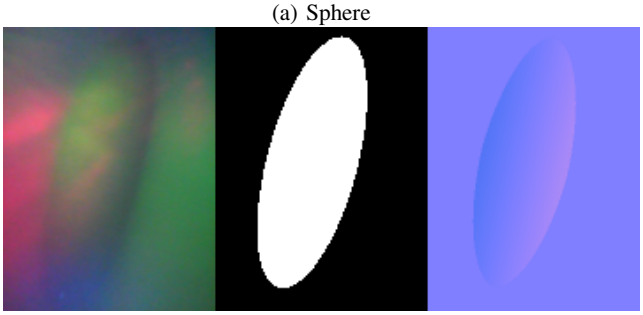

(b) Cylinder

Fig. 8: The image as taken by the sensor (left) with its corresponding ground truth for the contact model (middle) and depth model (right).

3) Training: Each DIGIT sensor uses a different internal LED lighting configuration as shown in Figure 9, so each model must be trained separately. The external lighting conditions are also critical for the accuracy of the sensor. Therefore, it is essential to include a sufficiently large dataset that captures a wide range of lighting variations or, if possible, maintain controlled lighting conditions.

Sensor D20791's contact model is trained using 264 images, while the depth model is trained using 230 images. The difference of 34 images is due to deformations caused by a flat circular shape, which the depth model cannot detect, as the entire deformation area has a normal vector of $[0, 0, 1]$ pointing straight down. This results in 5,068,800 data points for the contact model and 4,416,000 for the depth model. The data is split into training and testing sets with an 80/20 ratio, resulting in a training time of approximately 40 minutes.

The depth estimation model is trained using a mean squared error (MSE) loss function to regress per-pixel surface normals. Likewise, the contact model is trained with a binary cross-entropy loss function with logits (BCEWithLogits) to

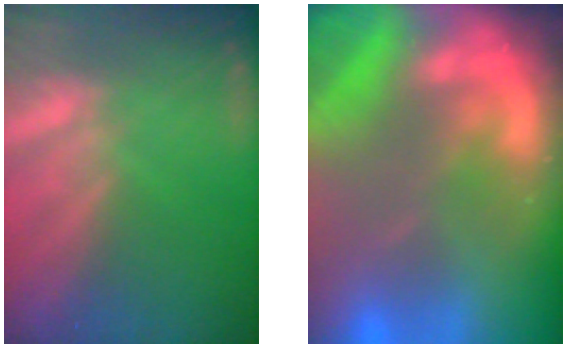

(a) Sensor D20791 (b) Sensor D20883

Fig. 9: Background images without any deformation showcasing the completely different internal lighting setup present for each sensor.

predict a binary contact mask for each pixel. This loss function includes a weighting factor to compensate for the dataset's imbalance between positive and negative samples.

4) Post Processing: The raw outputs of the depth and contact models require additional processing steps to ensure that the data is consistent, physically meaningful, and usable for downstream control logic.

a) Depth Model: The depth estimation network outputs a normal map, which can be converted to gradients using Equation 14, which is then converted into a depth map through Poisson surface reconstruction [21].

This depth map represents the distance from the gel surface to the camera. To produce a physically meaningful deformation map, the predicted distance is subtracted from the reference camera distance and then scaled by the thickness of the elastomer layer, which defines the maximum measurable deflection. The resulting map is clipped to the range [0,1] to eliminate values outside the expected deformation limits. To estimate the location and orientation of the contact, contours are extracted from the depth map to approximate the deformation profile.

$$\frac{dz}{dx} = -\frac{n_x}{n_z} \quad \text{and} \quad \frac{dz}{dy} = -\frac{n_y}{n_z} \tag{14}$$

The system performs a background calibration step to compensate for model error and any initial surface irregularities. This is achieved by computing an initial reference depth map as the average of the first 20 frames recorded by the sensor before contact occurs. The reference is then subtracted from all subsequent depth maps to correct for static offsets and ensure that only actual contact-induced deformations are retained.

b) Contact Model: The contact detection model outputs a per-pixel logit representing contact using a neural network. A Gaussian blur is applied to the logit map to reduce noise and incorporate contextual information from surrounding pixels. A sigmoid function then proceeds to convert the logit into a probability. A fixed threshold then converts this probabilistic map into a binary contact mask. This threshold is selected to minimize false positives, which are more detrimental to downstream control than occasional false negatives. Pixels with probabilities above the threshold are classified as contact points, while all others are set to zero. Principal Component Analysis (PCA) is applied to the resulting contact region to estimate the centroid and orientation of the contact patch, which informs the control logic.

Flowcharts summarizing the complete data pipeline for depth estimation and contact detection models are provided in Figure 10 and Figure 11, respectively.

B. Perching Control Strategy

The perching controller is implemented as a finite state machine (FSM) that sequences the drone through discrete flight and interaction phases. The FSM monitors motor states, odometry, and tactile feedback signals to make decisions at runtime. The controller combines autonomous search, contact detection, local pose adjustment, alignment correction, and final validation for the most complete experiment.

1) Initialization and Takeoff: The system starts in the `IDLE` state, initializing the gripper servos and opening the fingers. Once all motors are ready, a signal activates the optical tactile sensors. When both systems are prepared, the controller publishes the initial flight pose and transitions to the `TAKEOFF` state.

2) Search and Contact Detection: After reaching the initial setpoint, the FSM enters the `SEARCH` state. In this phase, the drone executes a predefined pattern by shifting laterally and stepping vertically in a zigzag pattern. The optical tactile sensors stream deformation magnitude and contact angle measurements at each step. If no contact is detected, the search continues for a maximum number of steps, after which the mission is aborted.

If any sensor force exceeds a defined threshold, the controller records the sensor ID and magnitude, then transitions to the `TOUCH` state.

3) Touch Alignment: In the `TOUCH` state, the drone adjusts its local pose based on which sensor made contact. For example, if contact is detected on a side sensor, the drone shifts laterally to better align with the target bar. After computing and publishing this new setpoint, the drone executes a slow press motion normal to the surface to confirm contact with the base sensor.

4) Alignment Correction and Yawing: After the pressing phase, the controller transitions to the `ALIGN` state. Here, it repeatedly samples the contact angle (bar orientation) from the base tactile sensor and computes the required yaw correction. If the detected misalignment exceeds a preset margin, the drone executes a yaw rotation (`YAW` state) until the bar orientation falls within tolerance. If the alignment remains outside acceptable limits after correction, the drone switches back to the `ALIGN` state.

5) Perching and Validation: Once the yaw alignment is within bounds, the FSM transitions to the `PERCH` state. At this point, the drone switches from position control to velocity control to avoid actively resisting the contact forces

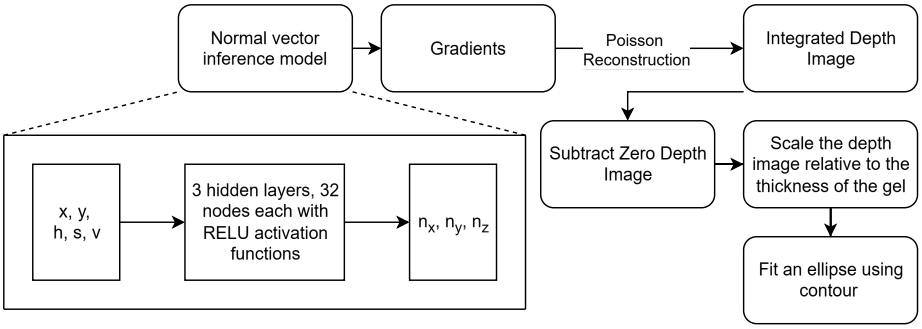

Fig. 10: Depth estimation model processing pipeline. The inference model outputs a normal vector, which is used to compute surface gradients. Poisson reconstruction is then applied to obtain the depth map. A zero-depth baseline is subtracted to reduce model error, and the result is scaled to the range $[0, 1]$ using the estimated thickness of the gel layer. Finally, contours are extracted, and an ellipse is fitted to the largest one to estimate the contact region.

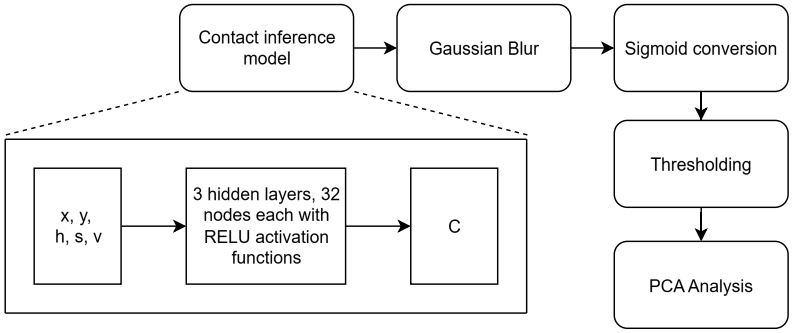

Fig. 11: Contact detection model processing pipeline. The inference model outputs raw contact logits, which are smoothed using a Gaussian blur before being converted to probabilities via a sigmoid function. These probabilities are then thresholded to produce a binary contact map. Finally, PCA is applied to the binary mask to estimate the location and orientation of the deformation.

during the perching maneuver. The gripper servos are then commanded to close around the bar. To ensure a stable attachment, the system checks that all fingertip tactile sensors report a sustained contact force above their predefined threshold. Additionally, a final manual perch confirmation can be provided through a user interface. If the validation conditions are met, the drone reduces its motor thrust to test the perch connection. Finally, it transitions to the `FINISH` state, where the fingers are reopened to release the bar and the drone executes a controlled, slow landing while remaining in velocity mode.

V. Results and Discussion

This section presents the key results from experiments. It highlights the performance of the contact and depth estimation models, the sensor's orientation estimation capabilities and the control strategy's behavior during flight tests.

A. Verification and Validation of the Sensor Models

To ensure that the developed normal and depth estimation pipeline works as intended, a series of verification and validation checks are conducted using a test dataset and deformation images obtained from the test site. These tests compare the predicted normal vectors and depth maps against known ground truth shapes and expected contact patterns. The goal is to verify the correctness of the implementation, evaluate the model's accuracy under representative conditions, and demonstrate its practical capability for detecting and quantifying contact on the DIGIT sensor.

1) Contact Model Verification: The performance of the trained contact model is evaluated on an independent test dataset using the BCEWithLogitsLoss, which averaged 0.2714. The output distribution for the predicted contact probabilities, shown in Figure 12a, demonstrates that the model effectively distinguishes between contact and no-contact regions. This is further supported by the receiver operating characteristic (ROC) curve, which achieved an area under the curve (AUC) of 0.9449. For this application, false positives are more problematic than false negatives, as they can incorrectly shift the estimated deformation to a region where no contact exists. False negatives, by contrast, merely leave occasional gaps in the predicted contact area. To favor precision over recall, a conservative threshold of 0.7 is applied to the probabilistic output when generating the binary mask, reducing the likelihood of false positives while accepting some gaps in the contact prediction. The final model thus reaches an overall accuracy of 0.8413, with a precision of 0.9703 and a recall of 0.8213, resulting in an

F1-score of 0.8896.

2) Depth Model Verification: The depth model demonstrates strong overall performance, with an average weighted MSE loss of 0.0022 when utilizing the testing dataset. The residuals for the n_x and n_y components are symmetrically distributed around zero, which, combined with high R^2 and explained variance values, indicates consistent and unbiased predictions across a wide range of input conditions. The normal component n_z shows a very low error, but this is partially due to the dominance of background pixels and minor deformations where the surface normal is nearly vertical. As a result, the model frequently predicts $n_z \approx 1$, leading to a less Gaussian residual distribution and comparatively lower R^2 and explained variance scores. The residual errors for each component are presented in Figure 13a.

TABLE II: Depth Model Quantitative Evaluation Metrics on the Test Dataset

Component	MAE	MSE	RMSE	R^2	Expl. Var.
n_x	0.0725	0.0116	0.1078	0.7630	0.7649
n_y	0.0668	0.0108	0.1040	0.7742	0.7748
n_z	0.0337	0.0035	0.0589	0.5443	0.5443

The network is not explicitly constrained to produce unit vectors; however, this is inconsequential, as the relative ratios between normal components, specifically n_x/n_z and n_y/n_z, are used to reconstruct the depth surface, as shown in Equation 14. The predicted ratio plotted against actual ratios, as shown in Figure 13b, confirms the model's reliability within the typical value range (-0.7 to 0.7) and demonstrates that it accurately predicts the direction of deformation. However, in high-slope regions where the true ratio approaches ± 1 or beyond, the model tends to underestimate the steepness, typically saturating around ± 0.7.

3) Validation: To evaluate the generalization capability of the trained models on unseen data, validation is performed using full-frame sensor images that are not part of the training dataset. Figure 14 shows representative results for three scenarios: a blank background image, and two real deformations caused by a cylindrical bar placed in both horizontal and vertical orientations.

In the background case, the contact model successfully identifies the absence of contact, producing a mostly blank mask with some false positives. The depth model outputs a flat map, as expected in the absence of deformation. In contrast, both deformation cases clearly highlight the differences in sensitivity and behavior between the two models. The contact model accurately identifies the full contact patch. Meanwhile, the depth model localizes the deformation more conservatively, focusing on the region of highest displacement.

These results highlight the strengths and trade-offs of each sensor model. The contact model is highly sensitive and capable of capturing a broader contact area, but it is more susceptible to false positives. The depth model provides more physically grounded and detailed measurements but requires greater indentation force to activate due to its lower sensitivity.

4) Base Sensor Angle Estimation: To further evaluate the accuracy of the base-mounted tactile sensor and validate its normal vector outputs, a series of controlled ground tests are performed. An OptiTrack motion capture system is used to measure both the attitude of the drone and the precise orientation of a calibration bar. During each test, the bar is pressed firmly onto the base-mounted DIGIT sensor while the drone is held stationary on the ground. This procedure established a known reference contact orientation, which is then compared to the sensor's predicted orientation to assess alignment errors and possible bias in the normal estimation pipeline.

The results of this experiment are shown in Figure 15. They indicate that, in general, the sensor performs well at angle estimation, though it occasionally produces significant errors. Considering all data, the mean absolute error (MAE) is 13.61°. However, when the RANSAC algorithm is used to detect and remove outliers, the MAE drops to 5.32°. The resulting trendline follows the equation $y = 0.87x + 1.49$, indicating a small positive bias of 1.49° and a tendency to slightly underestimate angles.

B. Flight Results

To evaluate the effectiveness of the proposed perching system in flight, a series of controlled tests are carried out in a laboratory environment. These experiments focused on validating both the accuracy of the tactile sensors and the drone's ability to perch securely on cylindrical targets.

Since contact forces are much harder to generate at the fingertips due to the large moment arm in an open configuration, the more sensitive contact model is used on them, while the base sensor, which can sustain higher forces, runs the depth estimation model.

However, the DIGIT sensor's elastomer surface is found to be too rigid to deform significantly under the contact forces encountered during flight. As a result, all experiments are conducted using simulated sensor output to validate the perching control logic. Additional details regarding this issue and other sensor-related limitations are provided in the Appendix I.

The perching trials are conducted using a metal bar, a plumbing pipe or a natural branch suspended horizontally parallel to the y-axis in midair to replicate typical cylindrical structures found in outdoor environments. This setup is shown in Figure 16. The drone approaches the bar autonomously and engages the grasping mechanism to secure itself around the target structure. The position and orientation of the drone are inferred using the OptiTrack motion capture system, allowing for accurate evaluation of the control strategy and the stability of the grasp under realistic conditions.

To focus on particular aspects of the drone individually, three different experimental variants are designed using the state machine outlined in subsection IV-B.

In the baseline experiment **without tactile feedback**, the `SEARCH`, `TOUCH`, `ALIGN`, and `YAW` phases are omitted.

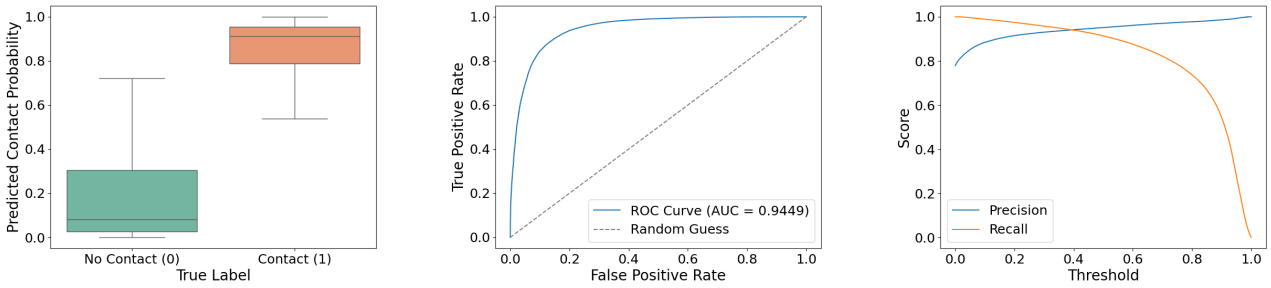

(a) Predicted contact probabilities (b) ROC curve (c) Precision–Recall curve

Fig. 12: Verification results for the contact model on the test dataset. **(a)** shows the distribution of predicted contact probabilities, indicating that the model confidently distinguishes between contact and non-contact regions. **(b)** presents the ROC curve with a large area under the curve (AUC), reflecting excellent separability. **(c)** displays the precision–recall curve, which supports the selection of a threshold of 0.7 to maximize precision while maintaining reasonable recall.

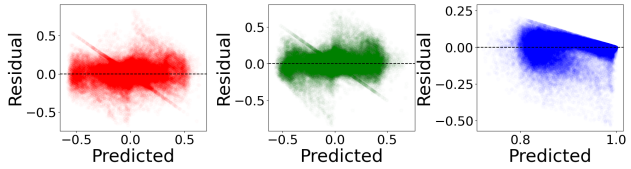

(a) Residuals for n_x, n_y, and n_z components.

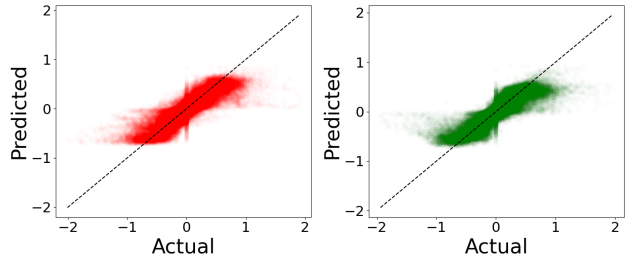

(b) Predicted vs actual slopes for n_x/n_z and n_y/n_z.

Fig. 13: Verification results for the depth model. **(a)** shows the distribution of residuals for each surface normal component on the test set. Residuals for n_x and n_y are almost symmetrically distributed around zero. The n_z residuals are more skewed due to the dominance of background regions with nearly vertical normals. **(b)** compares predicted and actual slope ratios n_x/n_z and n_y/n_z, which are used to reconstruct the depth surface. The model performs well for smaller slopes, but tends to underestimate steeper slopes.

Instead, the FSM transitions directly from takeoff to a predefined perch position before closing the gripper. To ensure the fingers do not collide with the bar, the drone first moves to a setpoint below the branch and then ascends to the correct perch position.

In the second variant, which **uses tactile feedback but assumes correct initial alignment**, the drone executes a search pattern and performs local position adjustments based on touch detection but skips the yaw correction logic. In this case, the `ALIGN` and `YAW` states are disabled. Once contact is

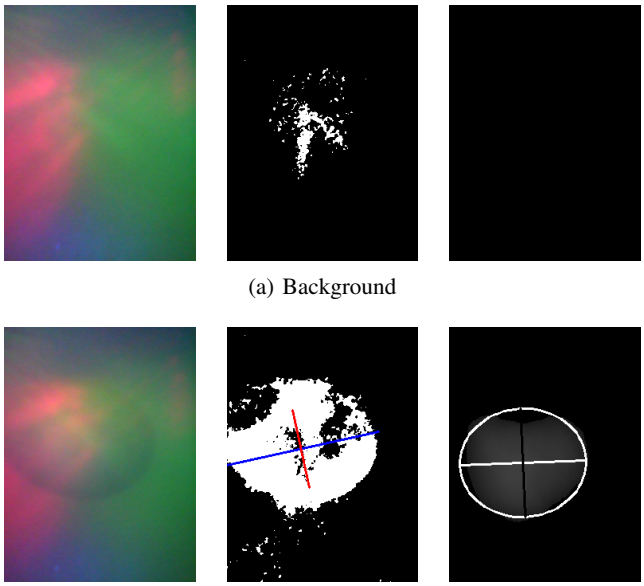

(a) Background

(b) Horizontal

(c) Vertical

Fig. 14: Validation results for three representative cases: (a) Background, (b) Horizontal Bar Deformation, and (c) Vertical Bar Deformation. Each row shows the raw RGB image (left), the predicted contact mask (middle), and the computed depth map (right).

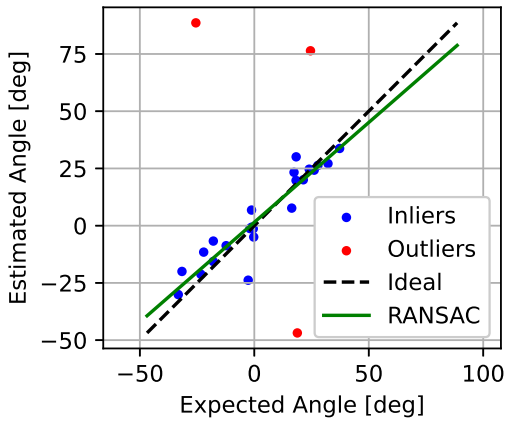

Fig. 15: Base sensor angle estimation results. A RANSAC algorithm is used to identify inliers and outliers, and a trendline with equation $y = 0.87x + 1.49$ is fitted to the inliers. The model exhibits a small positive bias and a tendency to underestimate angles.

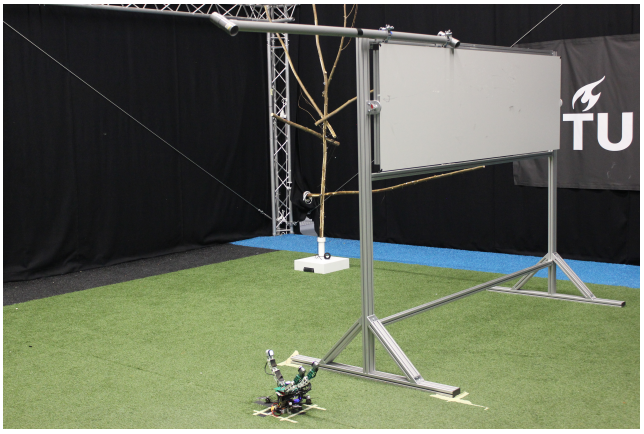

Fig. 16: Drone Perching Experimental Setup to simulate a branch or bar suspended in midair.

secured and the pressing phase completes, the FSM proceeds directly to PERCH.

In the final variant, which **utilizes tactile feedback to correct misalignments**, the drone is provided with the correct position of the branch and therefore skips the SEARCH and TOUCH states. It performs yaw corrections based on tactile feedback during the ALIGN and YAW states before proceeding to PERCH. As in the baseline experiment, the drone first moves to a setpoint below the bar before ascending.

As outlined in subsection IV-B, three experiments are performed. Fifteen runs of the experiment without tactile sensing are conducted to evaluate gripper stability and reach. The results are shown in Figure 17. The data indicates that the gripper is robust to position errors, successfully perching at offsets up to 0.12 m from the branch. The theoretical limit is estimated as the distance from the top of the base sensor

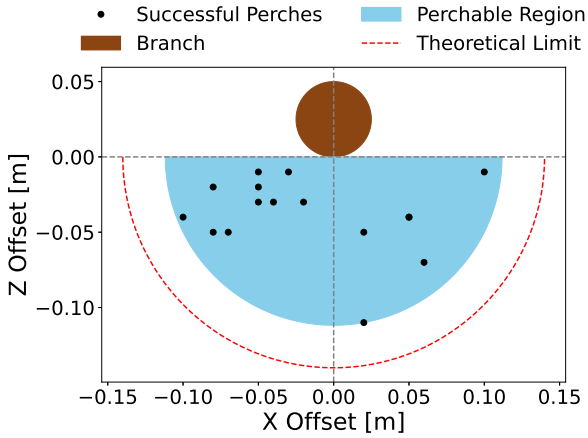

Fig. 17: Successful perching offsets in the XZ plane for 15 runs without tactile feedback. Each point represents the location where the drone attempted to perch relative to the branch. The results demonstrate the gripper's robustness to positional errors. The dashed boundary indicates the estimated theoretical limit defined by the reach from the top of the base sensor to the top of the second phalange.

to the top of the second phalange, beyond which the first phalange can no longer hook onto the bar and pull it into place. This distance is measured to be 0.14 m.

The second experiment is performed with the correct initial alignment but an incorrect position. Figure 18 shows the logs of two representative runs. These runs differ slightly: in Flight 1, the drone initially moves in the negative x-direction, while in Flight 2 it moves in the positive x-direction. As a result, Flight 1 detects (simulated) contact on the left sensor and adjusts leftward, whereas Flight 2 detects contact on the right sensor and adjusts rightward. In both cases, the drone uses the known positions of the fingertip sensors relative to the base sensor to correct its position and successfully perch.

The setpoint boundaries are shown, indicating the x-positions of the provided position setpoints. The z-position is increased in small increments until contact occurs. It is observed that the given x-direction setpoints are generally overshot by the drone. The setpoint boundaries are also used to illustrate the drone's reach and to define the zone in which the branch must be located for successful detection and perching.

The third experiment is conducted with the correct position setpoint but incorrect initial alignment. Figure 19 shows logs from three flights that performed orientation correction. The plots are time-shifted such that the transition to the yaw correction phase occurs at $t = 0$.

In all flights, an initial disturbance is observed due to the weight imbalance caused by the open-finger configuration. After stabilizing, the drone performs micro-adjustments beneath the bar. It then ascends and presses against the bar, and once the simulated required yaw angle is received, it corrects its orientation and completes the perch.

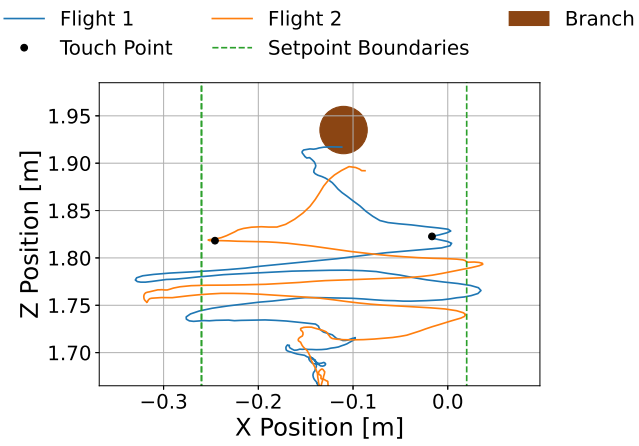

Fig. 18: Flight logs demonstrating position correction. At a height of 1.7 meters, the drone enters `SEARCH` mode. The setpoints given are in a zigzag pattern, and their x-positions are shown with the green dashed lines. Upon contact detection, it shifts to the correct perch position.

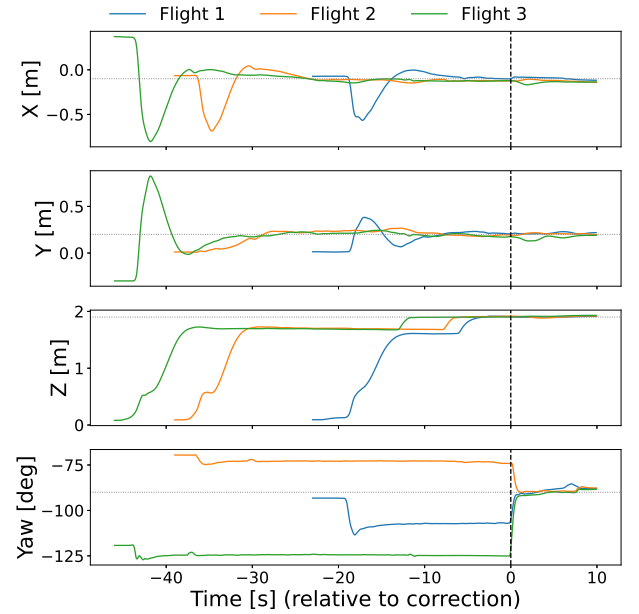

Fig. 19: Flight logs demonstrating orientation correction aligned such that the yaw correction occurs at $t = 0$. Each flight begins with an initial disturbance due to weight imbalance, followed by small adjustments beneath the branch. The drone then presses into the branch and corrects its orientation to align with it.

VI. Conclusion

This paper presents a grasping drone equipped with an underactuated gripper and high-resolution optical tactile sensors. A control strategy combining position and tactile feedback is developed to enable robust perching on cylindrical structures. Due to the rigidity of the DIGIT sensor's elastomer surface, simulated tactile data is used to evaluate the control system.

Two inference models are trained to process tactile images: a contact model for binary contact detection and a depth model for estimating surface normals. After outlier filtering, the depth model achieves a mean absolute error of $5.32°$ in angle estimation. Experimental results show that the gripper can successfully perch without tactile feedback despite small position errors. In the case of the designed drone, this tolerance extends up to 12 cm. However, in this case, the initial orientation needs to be correct. With tactile sensing, by contrast, the system can start anywhere within its horizontal reach and still eventually locate the branch, correcting both position and orientation errors. These findings demonstrate how tactile sensing enhances the drone's perching capabilities.

Overall, the results show that tactile sensing enables reliable aerial perching in uncertain conditions and lays the foundation for future improvements. Key directions for further development include modifying the sensor's hardware to be more compliant, or integrating other softer tactile sensors, integrating onboard visual sensing to eliminate reliance on motion capture, developing more advanced perception models with higher processing rates, adapting the gripper to a wider range of geometries, and validating the system in realistic outdoor environments.

References

[1] Fabio Ruggiero, Vincenzo Lippiello, and Anibal Ollero. "Aerial manipulation: A literature review". In: *IEEE Robotics and Automation Letters* 3.3 (2018). Publisher: IEEE, pp. 1957–1964.

[2] Jiawei Meng et al. "On aerial robots with grasping and perching capabilities: A comprehensive review". In: *Frontiers in Robotics and AI* 8 (2022). Publisher: Frontiers.

[3] Hanna Yousef, Mehdi Boukallel, and Kaspar Althoefer. "Tactile sensing for dexterous in-hand manipulation in robotics—A review". In: *Sensors and Actuators A: Physical* 167.2 (2011), pp. 171–187. ISSN: 0924-4247. DOI: https://doi.org/10.1016/j.sna.2011.02.038. URL: https://www.sciencedirect.com/science/article/pii/S0924424711001105.

[4] Karen Bodie et al. "An Omnidirectional Aerial Manipulation Platform for Contact-Based Inspection". In: *CoRR* abs/1905.03502 (2019). URL: https://arxiv.org/abs/1905.03502.

[5] Salua Hamaza, Ioannis Georgilas, and Thomas Richardson. "Energy-Tank Based Force Control for 3D Contour Following". In: *Towards Autonomous Robotic Systems*. Ed. by Kaspar Althoefer, Jelizaveta Konstantinova, and Ketao Zhang. Cham: Springer International Publishing, 2019, pp. 41–51. ISBN: 978-3-030-23807-0.

[6] Anish Jadoenathmisier. "Aerial Perching via Active Touch: Embodying Robust Tactile Grasping on Aerial Robots". In: *MSc Thesis, Delft University of Technology* (Dec. 2023).

[7] Liming Zheng and Salua Hamaza. "ALBERO: Dynamic Aerial Landing on Branches for Environmental Robotics Operations". In: *IEEE Robotics and Automation Letters* (2023). Publisher: IEEE.

[8] Sanghyeon Park et al. "Lightweight high voltage generator for untethered electroadhesive perching of micro air vehicles". In: *IEEE Robotics and Automation Letters* 5.3 (2020). Publisher: IEEE, pp. 4485–4492.

[9] Hai-Nguyen Nguyen et al. "A passively adaptive microspine grapple for robust, controllable perching". In: *2019 2nd IEEE international conference on soft robotics (RoboSoft)*. IEEE, 2019, pp. 80–87.

[10] William RT Roderick, Mark R Cutkosky, and David Lentink. "Bird-inspired dynamic grasping and perching in arboreal environments". In: *Science Robotics* 6.61 (2021). Publisher: American Association for the Advancement of Science, eabj7562.

[11] Raymond Ma and Aaron Dollar. "Yale OpenHand Project: Optimizing Open-Source Hand Designs for Ease of Fabrication and Adoption". In: *IEEE Robotics & Automation Magazine* 24.1 (2017), pp. 32–40. DOI: https://doi.org/10.1109/MRA.2016.2639034.

[12] K. Zhang et al. "SpiderMAV: Perching and stabilizing micro aerial vehicles with bio-inspired tensile anchoring systems". In: *2017 IEEE/RSJ International Conference on Intelligent Robots and Systems (IROS)*. Vancouver, BC, Canada: IEEE, 2017, pp. 6849–6854. DOI: https://doi.org/10.1109/IROS.2017.8206606.

[13] Xinyu Guo et al. "Powerful UAV manipulation via bioinspired self-adaptive soft self-contained gripper". In: *Science Advances* 10 (2024), eadn6642. DOI: https://doi.org/10.1126/sciadv.adn6642.

[14] Zhanat Kappassov, Juan-Antonio Corrales, and Véronique Perdereau. "Tactile sensing in dexterous robot hands—Review". In: *Robotics and Autonomous Systems* 74 (2015). Publisher: Elsevier, pp. 195–220.

[15] Salua Hamaza, Ioannis Georgilas, and Thomas Richardson. "2D Contour Following with an Unmanned Aerial Manipulator: Towards Tactile-Based Aerial Navigation". In: *2019 IEEE/RSJ International Conference on Intelligent Robots and Systems (IROS)*. IEEE, 2019, pp. 3664–3669.

[16] Wenzhen Yuan, Siyuan Dong, and Edward H. Adelson. "Gelsight: High-resolution robot tactile sensors for estimating geometry and force". In: *Sensors* 17.12 (2017). Publisher: MDPI, p. 2762.

[17] Michael Lambeta et al. "DIGIT: A novel design for a low-cost compact high-resolution tactile sensor". In: *Conference on Robot Learning*. 2020, pp. 1–10.

[18] Nathan F. Lepora et al. "DigiTac: A DIGIT-TacTip Hybrid Tactile Sensor for Comparing Low-Cost High-Resolution Robot Touch". In: *IEEE Robotics and Automation Letters* (2022). DOI: https://doi.org/10.1109/LRA.2022.3190641.

[19] Engineers Edge. *Coefficient of friction equation and table chart*. Publication Title: Engineers Edge - Engineering, Design and Manufacturing Solutions. URL: https://www.engineersedge.com/coeffients_of_friction.htm.

[20] Lorenz Meier, Dominik Honegger, and Marc Pollefeys. "PX4: A node-based multithreaded open source robotics framework for deeply embedded platforms". In: *2015 IEEE International Conference on Robotics and Automation (ICRA)*. 2015. DOI: https://doi.org/10.1109/ICRA.2015.7140074.

[21] Jack Doerner. *Fast Poisson Reconstruction in Python*. 2014. URL: https://gist.github.com/jackdoerner/b9b5e62a4c3893c76e4c.

APPENDIX I
LIMITATIONS OF THE DIGIT SENSOR

This appendix outlines the key limitations encountered when using the DIGIT sensor in the context of aerial perching experiments. Although the sensor provides high-resolution tactile data under ideal conditions, several challenges arose during practical integration with the drone platform. Two main limitations are discussed in this appendix: the lack of deformation of the contact surface under loads commonly experienced during flight, and the dimming experienced by the sensor cameras under certain conditions.

A. *Contact Surface Rigidity*

Throughout all experiments, the tactile sensors consistently failed to report any positive contact readings. Upon reviewing recorded flight data using logs, it is found that the sensor images showed almost no visible deformation. This held true even when the drone applied maximum available thrust, pressed directly against a branch (which has more texture and should be easier to detect), and is perfectly aligned at the center. As shown in Figure 20, the deformation remained minimal.

To validate this observation, a static experiment is conducted where the drone is placed on a scale, and the force required to produce detectable deformation on the base sensor is measured. It is found that approximately 30 N of force is needed when pressing with a metal bar and 20 N when pressing with a wooden branch. Given that the drone weighs about 1.2 kg and requires 60% of its thrust to hover, it has only about 10 N of thrust available for pressing.

These results confirmed that the contact forces encountered during flight are insufficient to meaningfully deform the DIGIT sensor's elastomer surface. As a result, all experiments in this thesis are performed using simulated tactile data.

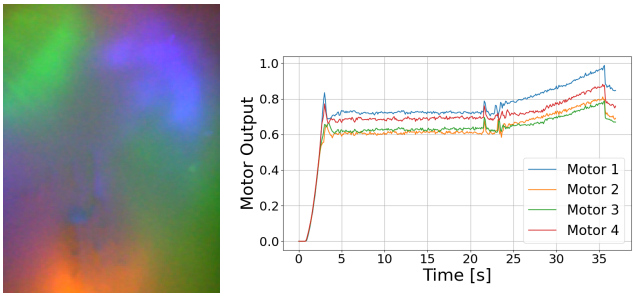

(a) Sensor Image (b) Thrust

Fig. 20: The maximum deformation observed during flight (left) despite full thrust (right) and ideal alignment

B. *Camera Dimming*

Another issue observed during experiments is the sudden dimming of the sensor camera under consistent lighting conditions, particularly after large deformations. As shown in Figure 21, images taken before and after deformation in a completely dark laboratory setting differ significantly in brightness, with the post-deformation image appearing much dimmer.

This dimming often led to false positives in the model, as most background images used during training are captured before deformation under normal lighting. Additionally, the dimming is non-uniform across the image, making it difficult to normalize or correct using standard preprocessing techniques.

The issue is more likely to occur after deformations involving reflective surfaces, such as metal bars, than more textured, diffuse surfaces like branches. It is also sometimes triggered if the sensors are initialized while the gripper fingers are closed, leading to reflections. As a mitigation strategy, the gripper is now kept open during sensor initialization to reduce the likelihood of this effect.

Simulating dimming in training data could potentially improve robustness, but due to the inconsistent magnitude and pattern of the effect, and the model's reliance on brightness as a key contact indicator, this approach has not yet been implemented. One possible explanation for the dimming is an automatic exposure adjustment by the sensor camera, although further investigation is required to confirm this.

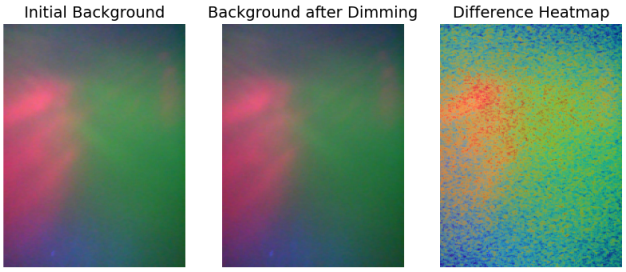

Fig. 21: (Left) Initial background before deformation; (Middle) dimmed background after deformation; (Right) pixel-wise brightness difference between the two.

3

Literature Study

Literature Study

By Muhammad Arham Elahi

Abstract— **Tactile sensing and perching mechanisms have gained increasing attention in the development of aerial robotics, aiming to enhance versatility, robustness, and energy efficiency. This literature study explores the integration of tactile sensors, particularly high resolution optical sensors, to improve grasping and perching capabilities in drones. The study investigates state-of-the-art tactile sensing technologies, their benefits and drawbacks, and their proven applications in ground-based robotics. It further reviews innovative gripper designs as well as unique drone-mounted perching strategies that offer lightweight, efficient solutions for autonomous operation. By analyzing advancements and limitations in both tactile sensing and drone perching technologies, this work identifies significant opportunities for improving drone autonomy and stability, bridging the gap between aerial and ground-based robotic systems. Applications range from energy-saving perching for environmental monitoring to precision agriculture, marking a step toward more capable and adaptive aerial systems.**

I. INTRODUCTION

In the rapidly evolving field of drone technology, versatile machines increasingly serve critical roles in domains such as precision agriculture, environmental monitoring, and infrastructure inspection [1, 2]. Traditional drones excel in passive tasks like surveying and image capture, but recent advancements emphasize developing drones capable of active physical interactions with their surroundings. This progression drives the development of aerial manipulators—drones equipped with robotic appendages that perform complex tasks, including grasping objects, manipulating tools, and perching on surfaces [3]. Aerial manipulators provide the benefit of a larger workspace compared to ground-based robots; however, their operation requires significantly more complex control systems. Maintaining stability poses a critical challenge because forces and moments cannot transfer to the ground, which necessitates advanced mechanisms to achieve precision and reliability.

Among the many capabilities of aerial manipulators, perching attracts considerable attention. This ability enables drones to attach to the environment, conserving energy and enhancing task stability during operations such as long-term monitoring or inspection [4]. Achieving robust perching, however, involves several challenges, including regulating contact forces, correcting orientation, and maintaining interaction precision. These challenges emphasize the importance of advanced sensing technologies to supplement conventional vision-based methods, particularly in low-visibility environments.

Tactile feedback emerges as a promising modality in robotics for enhancing interaction precision. By mimicking the human sense of touch, tactile sensors deliver detailed information about physical interactions, including force, texture, and stiffness [5]. In aerial manipulators, tactile feedback provides notable advantages, such as detecting and adjusting to object slippage, determining object orientation, and guiding grasp configurations through tactile servoing. This capability allows drones to perform precise, real-time adjustments based on environmental feedback, improving their effectiveness in object manipulation and compliant grasping tasks.

Tactile feedback, though widely successful in ground-based and industrial robotics, remains underexplored in aerial robotics. Research has shown the potential of force sensors in aerial manipulators for tasks such as contour following and force regulation [6, 7]. However, understanding the full range of applications for tactile feedback, particularly in autonomous perching scenarios, remains incomplete. Challenges like occlusion caused by grippers or low-light conditions, which frequently hinder vision-based systems, can be effectively mitigated through tactile sensing [8]. During manipulation, vision-based systems often suffer from inherent occlusions that tactile sensors can naturally overcome, highlighting the complementary nature of these two modalities.

This literature study examines the integration of the advanced tactile sensor DIGIT into a perching drone currently equipped with binary capacitive sensors. The study begins with an overview of the research background in section II, followed by a discussion on the current state of the art in section III. A detailed analysis of the DIGIT sensor and its capabilities appears in section IV. Finally, the challenges and opportunities associated with the project are addressed in section V, and the study concludes in section VI.

II. BACKGROUND

This report builds on a previous iteration of a grasping drone design [9]. The earlier design featured a quadcopter equipped with a three-fingered grasping mechanism. Each finger was underactuated to ensure inherent compliance, controlled by three servos per finger, and designed with three degrees of freedom—mimicking the structure of a human finger. Tactile feedback was provided by Adafruit MPR121 capacitance sensors embedded in the phalanges, functioning as binary touch detectors. However, these sensors were limited to detecting contact with conductive materials [10]. A render of the drone design appears in Figure 1.

The grasping mechanism undergoes testing using a metal rod as the perching target. The drone follows a predefined elliptical or zigzag search trajectory to locate the rod. Upon making contact, it aligns itself such that the base of the

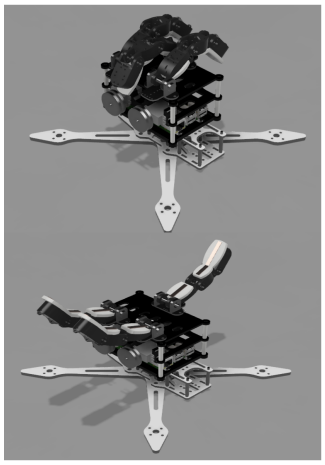

Fig. 1. A CAD render of the Original Perching Drone Design in both an closed (top) and open (bottom) configuration [9]

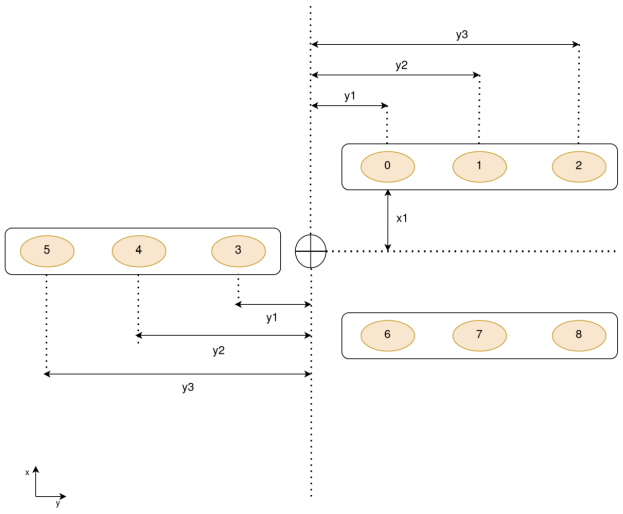

Fig. 2. The gripper configuration and the location of each sensor pad which maps $\mathcal{F}$ for all 9 sensor pads by taking the distances from the center

drone is in line with the rod, it acheives that by using the touch event to calculate the corresponding offset which allows for the computation of the goal position for the drone. Equation 1 shows the computation of $\hat{x}_{goal}$ when $\hat{x}_{touch}$ is the position of the drone at the touch event and $\hat{x}_{offset}$ is the adjustment based based upon the touch vector τ (an array of binary variables for the touch state of each pad). Figure 2 further demonstrate the conversion from τ to $\hat{x}_{offset}$ from the center. Once the drone is aligned, it executes a grasping maneuver, and then verifies it by checking whether the bottom pads on all three fingers register contact. If the attempt fails, the drone realigns itself with the rod and retries the grasp. Once a stable grasp is achieved, the drone shuts down its motors, allowing it to perch passively without consuming additional power. Images illustrating all the drone states appear in Figure 3.

$$\hat{x}_{goal} = \hat{x}_{touch} + \hat{x}_{offset} \quad \text{where} \quad \hat{x}_{offset} = \mathcal{F}(\tau) \quad (1)$$

To validate the drone's perching capabilities, multiple trials were conducted, with the drone employing either a zigzag pattern or an elliptical pattern to search for the target rod. Figure 4 presents the results of these trials. The zigzag pattern consistently demonstrates shorter average flight times and requires fewer attempts to perch successfully. Additionally, it results in fewer failed attempts, leading to the conclusion that the zigzag pattern is more efficient than the elliptical pattern for the given configuration and perching application. Figure 5 highlights the drone's ability to handle offsets and achieve a position relatively close to the target object when transitioning from an open state to a closed state after a touch event. Additionally, Figure 6 demonstrates a significant improvement in perching performance with the incorporation of tactile sensing. The experiment employs three y-offsets (0, 0.05, and 0.14), conducting five trials for both open-loop and closed-loop implementations. This setup results in a total of 15 trials per controller [9].

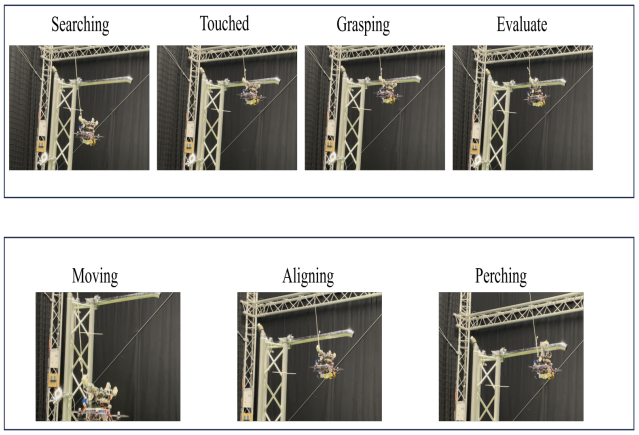

Fig. 3. The different Perching Drone States used in Jadoenathmisier et al. [9], the drone searches in a particular pattern until a touch event occurs, upon which a grasp is attempted and evaluated, if evaluation is successful drone starts perching otherwise it will move and realign before attempting another grasp and evaluating it

Despite its functional design, the system exhibits significant limitations. The capacitance sensors fail to provide information about the target's orientation, requiring the orientation to be predetermined before initiating the perching sequence. This reliance on precise pre-alignment limits the drone's flexibility and adaptability in dynamic environments.

To address these limitations, this report proposes integrating DIGIT sensors, a higher-resolution optical tactile sensing system [11]. These sensors capture detailed information about force distribution and contact deformation, enabling the drone to estimate both the position and orientation of the target object. This enhancement allows the drone to perform autonomous perching maneuvers, regardless of its initial orientation, greatly improving its versatility and effectiveness

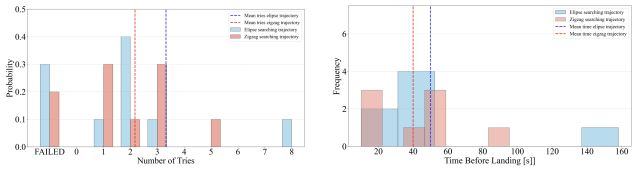

Fig. 4. Distribution plots comparing the perching performance using an elliptical path and a zigzag path. Each trajectory is assessed through 10 trials with distribution of the number of attempts before achieving a successful perch (left) and the distribution of the time taken to successfully perch (right) [9]

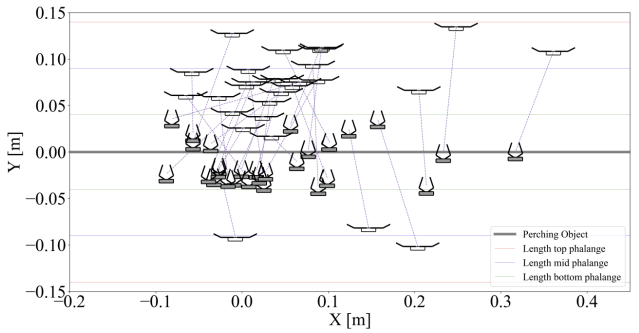

Fig. 5. The response following a touch event is shown, the drone transitions to an "open" state upon detecting a touch event, and to a "closed" state when attempting a grasp, which can be seen to consistently converge toward the bar [9]

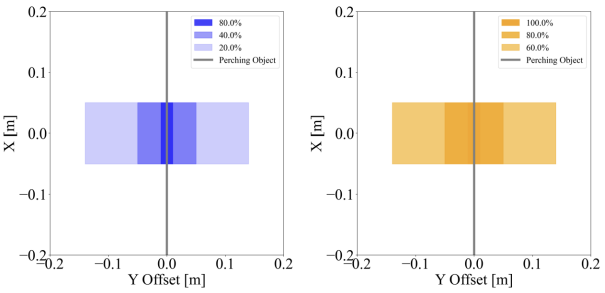

Fig. 6. The perching performance with (right) and without (left) tactile feedback is shown, the evaluation focuses on lateral (y) uncertainty in the perching object's position [9]

Fig. 7. The DIGIT sensor to be used in the new drone design, it will replace the existing capacitive tactile sensors [12]

in real-world applications. The DIGIT sensor appears in Figure 7.

III. State of the Art

A. Aerial Manipulators

Aerial manipulators represent a rapidly advancing field within robotics, combining the mobility of drones with the functional complexity of robotic manipulators. These systems suit tasks that require both precision and reach in environments inaccessible to ground-based robots or humans. Examples include Figure 8, which shows contact-based infrastructure inspection, Figure 9, which depicts the MHYRO drone performing object retrieval in hazardous areas, and Figure 10, which illustrates agricultural operations such as fruit picking or pruning.

The defining feature of aerial manipulators is their ability to actively interact with the environment, which requires a combination of lightweight manipulator designs and control systems. Early designs were simple, relying on rigid grippers for pick-and-place tasks [14]. However, the field has since evolved to include underactuated manipulators, which use fewer actuators than degrees of freedom to balance simplicity and adaptability. Advanced systems now incorporate fully actuated arms and compliant mechanisms that ensure precision in grasping while maintaining safety during interactions with delicate objects [15].

The integration of compliant grippers, inspired by biological systems such as elephant trunks and octopus tentacles, marks a significant milestone in aerial manipulation. These grippers use flexible materials or torsional springs to adapt to object shapes, enabling the safe handling of irregular or fragile items. Recent designs have also incorporated tunable stiffness, allowing aerial manipulators to switch between rigid and compliant behaviors as needed [15, 16].

Aerial manipulators face unique challenges related to flight dynamics, particularly in ensuring stability during manipulation. Unlike ground-based robots, they cannot rely on fixed supports to counteract forces and torques generated by the manipulator's movement, interactions with the environment, and aerodynamic effects. To address this, control algorithms must integrate the dynamics of both the drone and the manipulator, enabling precise control over position, orientation, and force application while maintaining stable flight [17].

Aerial manipulators encounter challenges due to the trade-off between payload capacity and manipulator functionality. This issue remains critical, as adding sensors or actuators increases weight and energy consumption. Environmental factors, such as wind or uneven surfaces, further introduce variability that complicates precise manipulation. These challenges emphasize the need for lightweight materials, energy-efficient actuators, and robust sensory systems to ensure reliable operation across diverse scenarios [15].

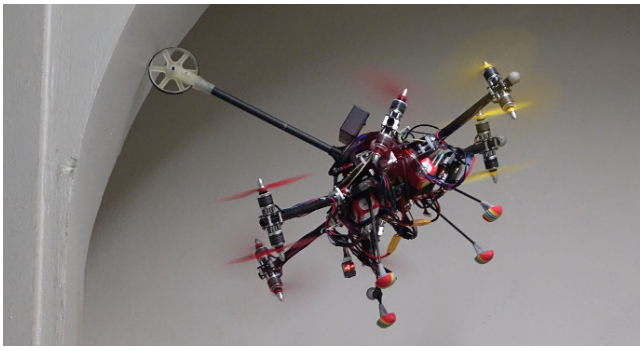

Fig. 8. A Contact-based Inspection Drone demonstrating a use case for aerial manipulators, uses a fully actuated tilt-rotor system [6]

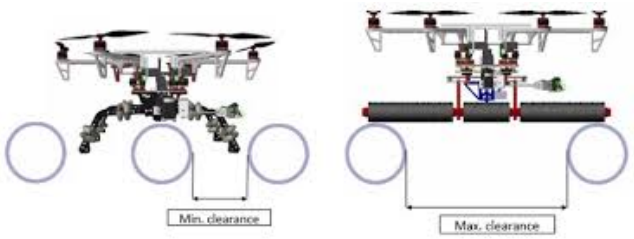

Fig. 9. Modular HYbrid RObot (MHYRO) Drone demonstrates another use case of aerial manipulators, reaching inaccessible locations, in this case either between a rack of pipes or on a singular pipe, depending on the landing gear attachment [13]

B. Perching Drones

Perching drones have emerged as a specialized area of aerial robotics, driven by the need for energy-efficient and stable operations in challenging environments. Unlike conventional drones, which must remain airborne while performing tasks, perching drones can attach to the environment, allowing for prolonged operations with reduced energy consumption. This capability proves particularly valuable for applications such as environmental monitoring, infrastructure inspection, and surveillance [8, 18, 19].

Perching drones integrate interaction capabilities through the use of grasping, attaching, or embedding technologies. Figure 11 shows the three methods.

Grasping is one of the primary methods of perching and draws inspiration from birds. It encompasses a wide range of designs, including grippers and robotic arms. To further enhance versatility, grasping technologies often employ reconfigurable frames with prismatic joints for linear extension and revolute joints for rotational adjustments [4].

For tasks that require temporary stabilization or secure interaction with surfaces, attaching technologies suit better. These can include magnets for attaching to ferromagnetic surfaces such as pipelines or steel infrastructure. Dry adhesives, inspired by the microscopic hairs on gecko feet, provide strong, reusable adhesion on smooth surfaces [20, 21]. Electrostatic adhesives generate electrostatic forces to adhere to surfaces without requiring specialized materials.

Fig. 10. A precision Agriculture Drone shows yet another use case for aerial manipulators, fruit harvesting [13]

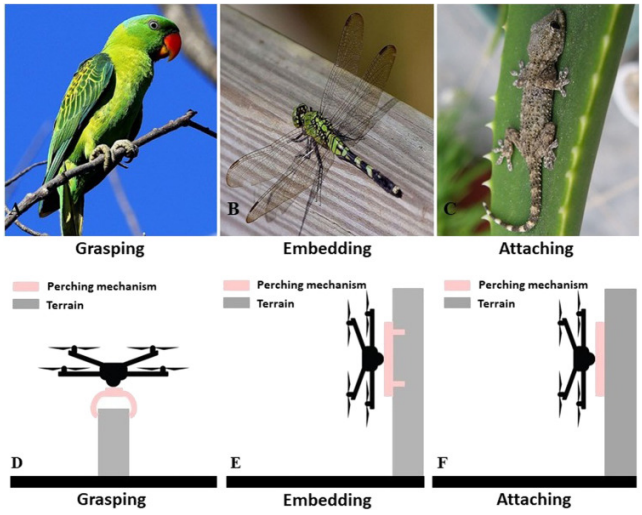

Fig. 11. The three main types of perching mechanisms, grasping, embedding and attaching - all inspired by biological mechanisms exhibited by birds, insects and lizards respectively [4]

Vacuum cups create a secure grip in environments where suction works, such as on flat or slightly curved surfaces. These technologies enable aerial manipulators to perch on vertical surfaces, cling to ceilings, or stabilize themselves during interaction [4].

Embedding technologies draw inspiration from nature, particularly insects, to achieve reliable attachment to irregular or textured surfaces. Insect-inspired spines, for instance, mimic the ability of insects to anchor themselves to rough or porous materials [22]. These technologies extend the range of environments in which aerial manipulators operate, making them highly effective in natural settings such as tree trunks or rock faces [4].

Perching mechanisms in drones can also categorize into passive and active systems. Passive mechanisms latch onto surfaces without requiring continuous actuation. These mechanisms include compliant gripper mechanisms, dry adhesives, and embedding technologies. Such designs remain lightweight and energy-efficient but may struggle with pre-

cision or adaptability to various surface types [8, 23]. Active mechanisms aim to achieve precise control during perching by utilizing energy throughout the perching process. They use technologies like actuated grippers and suit irregular surfaces better but introduce additional weight and complexity while also increasing power consumption [18, 19].

Since grasping serves as the primary method for perching mechanisms, and the previously developed drone also uses this approach, this report will give special attention to a few drones with similar designs. The report will then discuss unique designs that do not fall into the categories of grasping, embedding, or attaching.

1) Underactuated Compliant Gripper: The first example is the work done by the GRAB Lab at Yale through its OpenHand Project on gripper design. The final product features four fingers with eight degrees of freedom, which can be either underactuated or fully actuated, depending on the choice of fingers. When configured with four underactuated fingers, the design incorporates compliant flexure joints driven by a single actuator through a pulley differential mechanism. Figure 12 shows the final design [24, 25].

Although initially designed for ground-based robots, the gripper was later applied in a variety of contexts, including being mounted to the bottom of a helicopter and used to grasp cylindrical, circular, and planar objects, as the image in Figure 13 shows. Despite lacking tactile feedback, the gripper utilized its soft fingerpads and underactuated, compliant design to successfully carry objects weighing up to approximately 1.5 kg. The gripper design is modular, with most of its structure made of PLA material and rubber, making it highly cost-effective.

Researchers conducted further investigation on the design optimization of the prismatic-revolute-revolute (PRR) joint system used in the helicopter-mounted gripper. The findings suggested that the link lengths should decrease sequentially, with the first link being the largest and the fingertip link being the smallest. Additionally, they concluded that underactuated systems with one motor per finger suffice for the application. While a fully actuated system enhances the grasping capabilities, it also converts the gripper from a passive to an active grasping system, thus reducing efficiency [26–28].

2) Avian-Inspired Grippers: The second example features a perching drone with grippers mounted to its underside. This avian-inspired design incorporates two compliant, underactuated claws and two folding legs. The folding legs play a key role in the mechanism, as they use the drone's weight to generate tendon tension, enabling it to perch passively on branches and other cylindrical objects. The design and its influence appear in Figure 14. The perching mechanism remains extremely lightweight, which is essential for its ability to perch passively. The mechanism itself weighs only 478 grams, while the attached drone weighs 388 grams. Notably, this design does not incorporate tactile sensing or soft fingerpads. Instead, each individual toe cuts from a sheet of polyurethane using a waterjet, with notches added to create flexible joints. Hollow tubing on the underside of each toe segment allows for tendon routing [29].

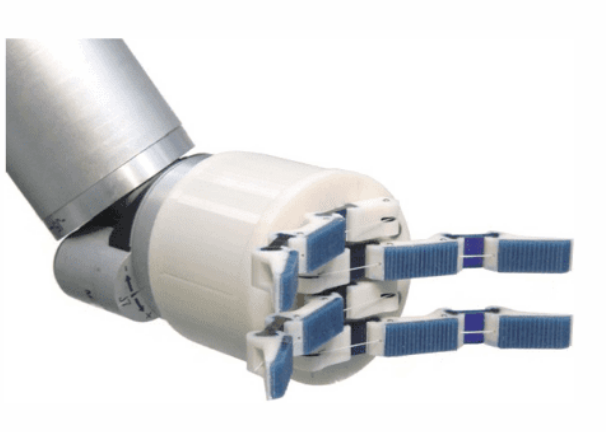

Fig. 12. The Yale OpenHand Gripper mounted to a ground-based robotic arm, it uses underactuated phalanges and soft fingerpads and is modular but does not utilize tactile sensing [24]

Fig. 13. Yale Gripper mounted below a helicopter and used for grasping a wide range of objects [24]

3) Anchor-based Perching: An example of a unique active perching mechanism is the SpiderMAV drone, which draws inspiration from the web construction and locomotion capabilities of arachnids. It shoots threaded anchors from launchers using high-pressure gas actuators, allowing the anchor to reach fixed structures from a distance and attach to targeted positions. It can also launch multiple anchors at once, enabling the drone to perch or create an extremely stable mode for tasks requiring a high degree of precision [19]. An image depicting the SpiderMAV drone appears in Figure 15.

4) Tendril-based Grasping: Another interesting drone design for grasping appears in the work by Guo et al. It draws inspiration from tendril plants and consists of two types of U-shaped soft eccentric circular tube actuators, one for delicate grasping and the other for strong grasping. The tubes are filled with a liquid that has a low boiling point; when a voltage passes through a wire, it heats the liquid sufficiently for it to transition into a gas. The resulting pressure increase causes the tubes to curl up and grasp any object within reach. This design allows for adaptable, powerful manipulation without

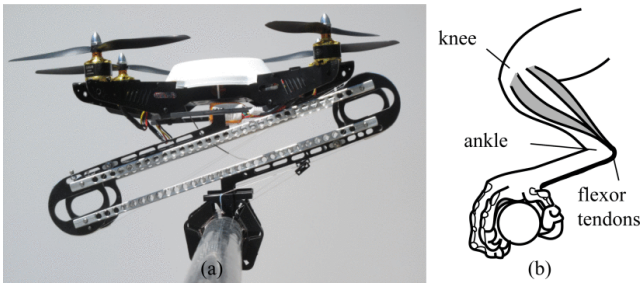

Fig. 14. An avian inspired perching mechanism which uses feet that are solely actuated by the drone's own weight [29]

Fig. 15. The SpiderMAV drone which shoots threaded anchors into fixed structures, allowing it to perch[19]

requiring complex grasping planning. However, the tradeoff is low positioning accuracy [23]. Figure 16 demonstrates how the mechanism works. Although the design has only been used for grasping, a sufficiently strong actuator and lightweight drone could enable it to be used for perching.

5) Challenges of Integrating Tactile Sensing: Sensing systems play a critical role in the further development of perching drones. Traditional perching drones rely on cameras or LiDAR for target detection and alignment, which, while effective in controlled environments, face challenges like occlusion, glare, or poor lighting [8]. This research explores the integration of tactile sensors to enhance perching precision. Tactile sensing provides real-time data on contact forces, enabling drones to adjust their grip or alignment autonomously. This approach addresses the limitations of vision systems, making it ideal for tasks in low-visibility conditions [11].

Despite significant progress, developers still face several challenges in the development of perching drones. Achieving a balance between lightweight design and robust functionality remains a persistent issue, as adding sensors or actuators increases the payload. Moreover, engineers must design grippers that can securely attach to a wide range

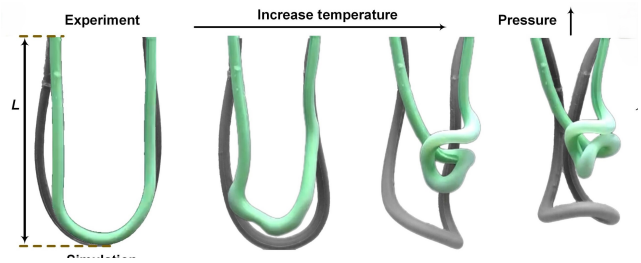

Fig. 16. A Tendril actuation mechanism which utilizes the temperature and pressure increase caused by a voltage change to grasp objects [23]

of surfaces, including smooth or moving targets, which presents a technical hurdle. Real-time data processing and the integration of vision and tactile feedback require advanced algorithms and control systems [8, 23].

6) Applications: The potential applications of perching drones are numerous. For instance, agricultural tasks like fruit harvesting or pruning would benefit from drones that perch on trees for stable operations. Similarly, drones designed for long-term environmental monitoring can conserve energy by perching between data collection intervals [18, 19].

C. Tactile Sensing

Tactile sensing represents a cornerstone of robotic innovation, allowing systems to perceive and interpret physical interactions with their environment. Unlike vision-based sensors, tactile sensors directly measure contact dynamics such as force distribution, texture, and deformation, enabling robots to adapt to tasks that require precision, compliance, or sensitivity to delicate objects. Historically, tactile sensing has played a central role in advancements in robotic manipulation, particularly in industrial and ground-based robotics. For example, the Gifu Hand 2, a robotic hand containing servomotors for each joint, features a six-axis force sensor at each fingertip, complemented by a distributed tactile sensor design over the rest of the surface [30]. It is shown in Figure 17. However, integrating tactile sensors into aerial systems remains an emerging field with substantial potential for enhancing performance in unstructured environments [5, 10]. This section provides a detailed breakdown of all major tactile sensing technologies and their properties, including resistive sensors, capacitive sensors, piezoelectric sensors, and optical sensors. The section also concludes by briefly addressing some other novel technologies.

1) Resistive Sensors: Tactile sensing technologies leverage various mechanisms, with resistive sensors being one of the most fundamental. A resistive sensor can employ configurations such as MEMS strain gauges and piezoresistors to measure force along specific axes with high sensitivity. These setups integrate seamlessly with other MEMS and electronics, offering compact and versatile solutions. Their working principle is quite simple, as the force is directly coupled to the strain measured in the gauges and can be computed with Equation 2 where k is the stiffness of the

Fig. 17. The Gifu Hand 2, an early demonstration of the benefit of tactile sensing in robotics, it utilizes six-axis fingerprint sensors while also containing a distributed tactile sensing system over the rest of its surface [30]

gauge and ϵ the strain measured. Figure 18 shows an example of such a sensor configuration. Despite their advantages, these sensors face several drawbacks, including fragility, high manufacturing costs, and limited flexibility or stretchability. Additionally, while the sensor itself may be small, the overall package often becomes bulky. To address these limitations, embedding the sensor in an elastomer has proven beneficial. The elastomeric layer mimics human skin, enhancing grasping quality and providing some degree of flexibility. However, this approach reduces sensitivity and introduces challenges such as creep over time [31–33].

$$F = k\epsilon \tag{2}$$

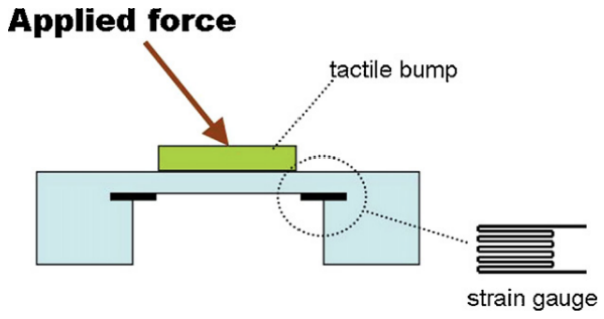

Fig. 18. Strain gauge and Piezoresistor Sensor Setup, any force applied to the tactile bump will result in deformation of the diagraphm and thus the strain gauges which can then be measured [31]

Another variation of resistive tactile sensors involves two layers of conductive polymer films separated by a highly porous and much less-conductive layer, such as foam. The working principle of this sensor is significantly more complicated, it is mainly related to the resistance of the interface between the electrodes and the film. Figure 19 shows that the roughness of the film leads to minimal contact area with the electrodes under zero load, however when a force is applied, the contact area increases significantly, thus resistance descreases. This relationship is highly nonlinear and needs to be calibrated precisely, but if done properly an area function $A(F) = [0, 1]$ can be defined. Equation 3 can then be used to express the electrical interface resistance R_S using the surface resistance of the sensor material R_{SO}. Equation 4 shows the total resistance which is just the summation of the R_S of the two electrodes and R_V the volume resistivity of the sensor material [34].

$$R_S(F) = \frac{1}{A(F)} R_{SO} \tag{3}$$

$$R(F) = 2R_S(F) + R_V \tag{4}$$

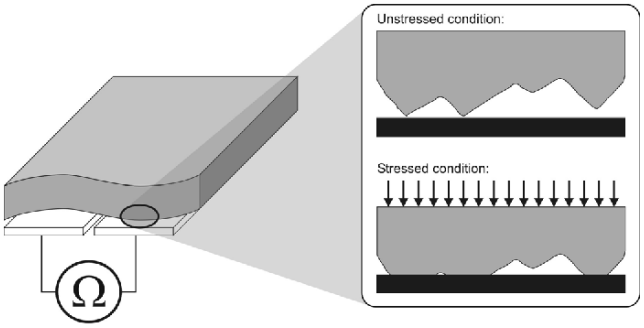

Fig. 19. Working Principle of a resistive sensor, the more pressure is applied, the higher the contact area gets, reducing the resistance of the electrode interface [34]

These sensors are cost-effective, robust, chemically resistant, and mechanically flexible, making them suitable for large-area applications. Nevertheless, they are not very stretchable, have low sensitivity, and are restricted to pressure sensing or imaging due to omnidirectional conductivity. Figure 20 shows an image of such a sensor. Conductive elastomer composites present another option, combining the flexibility of soft materials with improved grasping quality. While stretchable and capable of being tailored for specific measurement ranges, these composites are more expensive and may suffer from hysteresis during operation. Overall, these resistive sensors are relatively simple, cost-effective, and flexible. However, they depend heavily on proper calibration, particularly with respect to variations in temperature and moisture. They are prone to performance degradation over time and often exhibit non-linear responses [10, 31, 35–37].

One promising direction of research for resistive sensors involves modifying them to simultaneously detect both pressure and temperature. This can be achieved by constructing multimodal sensors through the stacking and layering of conductive rubber composites. Such a configuration enables the sensor to be sensitive over a wide range of temperatures and pressures while maintaining stretchability and low

manufacturing costs. However, further research is needed to explore the limitations and potential drawbacks of this approach, such as performance degradation, hysteresis, or sensitivity to other environmental conditions [38].

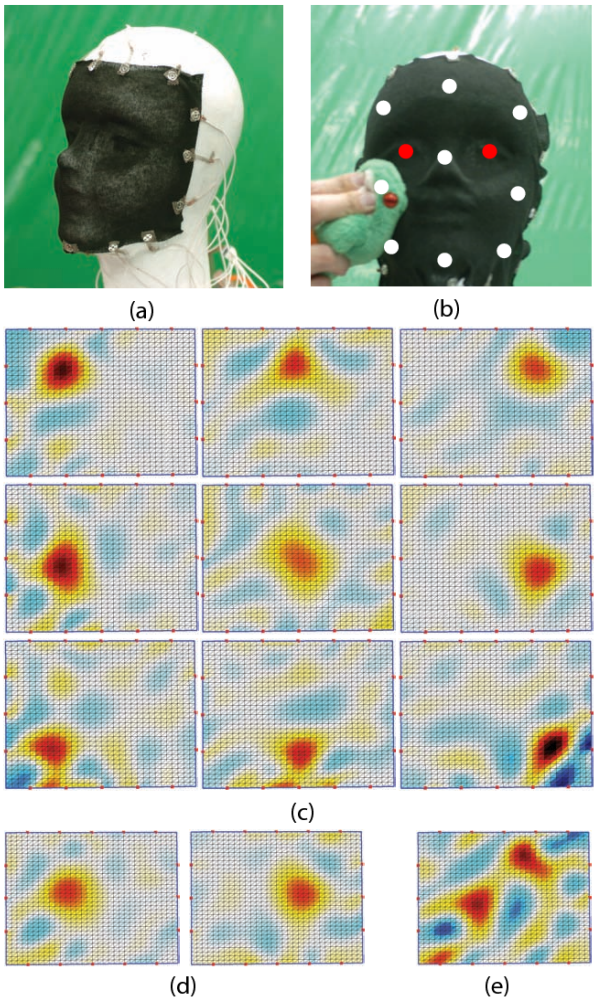

Fig. 20. A conductive polymer resistive sensor a) wrapped over a a dummy face b) white and red spots show the points were pressure is applied c) the corresponding results for the white spots d) the corresponding results for the red spots e) shows the results for applying force at two spots [39]

2) Capacitive Sensors: The second type of sensor to be discussed is capacitive sensors, which consist of two conductive plates separated by a compressible dielectric material. When the gap between the plates changes under applied forces, the capacitance varies. This working principle can be explained using the capacitance formula shown in Equation 5 where ϵ_0 is free space permittivity, ϵ_r is relative permittivity, A is the surface area and d_0 is the undeformed distance between the plates. Equation 6 shows how the formula is adapted for a deformed sensor, since the distance between the plates is no longer uniform, it needs to be integrated over the entire area while taking into account the diaphragm deflection $w(x, y)$ over the surface [40]. The change in this capacitance due to this deformation is usually quite small, only amounting to a few femto farads, therefore a complex signal conditioning electronic is needed for detection [34].

$$C = \epsilon_0 \epsilon_r \frac{A}{d_0} \tag{5}$$

$$C = \epsilon_0 \epsilon_r \int_{x=0}^{a} \int_{y=0}^{b} \frac{1}{d_0 - w(x, y)} dxdy \tag{6}$$

Capacitive sensors can achieve relatively high sensitivity depending on the compressibility of the dielectric material and the sensor's thickness. Unlike resistive sensors, capacitive sensors are temperature-independent, making them advantageous for applications in varying environmental conditions. They are versatile, suitable for both large-area applications (emulating skin) and small-scale setups (emulating fingertips). Additionally, they benefit from well-established manufacturing techniques and are more power-efficient compared to resistive sensors [10, 31, 36, 37].

Capacitive sensors are capable of measuring shear forces and thus forces in three dimensions by embedding multiple capacitors within the sensor, as Figure 21 illustrates. When embedded in an elastomer, capacitive sensors gain stretchability and softness, enhancing their grasping capabilities. However, this comes at the cost of reduced sensitivity, similar to resistive sensors. Despite their benefits, capacitive sensors have several drawbacks. They are highly susceptible to electromagnetic interference and, like resistive sensors, exhibit nonlinear responses and hysteresis. Additionally, they suffer from high data latency, making them less suitable for agile, real-time applications. Poor repeatability in manufacturing further complicates their implementation, requiring each sensor to be individually calibrated. They also suffer from parasitic capacitance introducing further noise and reducing their sensitivity. The complex circuitry required for their manufacture also lends itself to higher costs compared to resistive sensors [10, 31, 36].

Capacitive sensors rank among the most widely utilized tactile sensors in real-life applications, with touch screens exemplifying their practicality [10, 41]. In robotics, these sensors frequently appear in robotic hand designs, showcasing their effectiveness in replicating human-like dexterity [9].

Advancing capacitive tactile sensors focuses significantly on developing multi-modal systems. These systems integrate capacitive sensors with complementary technologies to address their individual limitations. For instance, incorporating triboelectric nanogenerators (TENG) into bimodal tactile sensors helps mitigate electromagnetic interference, a common drawback of capacitive sensors [42]. Despite these benefits, multi-modal systems face challenges such as high power consumption, complex data fusion, and real-time data transmission [43].

Enhancing the dielectric layer in capacitive sensors represents another key research direction. Researchers aim to replace traditional elastomer layers, which often experience performance degradation, hysteresis, and limited flexibility, with more robust materials. For example, thin 3D fabric layers inspired by textile manufacturing

techniques have been proposed as a flexible, durable, and scalable alternative. This approach addresses mechanical limitations while simplifying the manufacturing process [44].

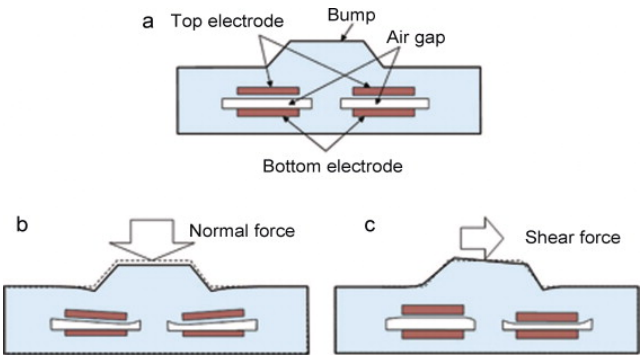

Fig. 21. The working principle for capacitive sensors for 2D measurement a) cross section of the sensor, an undeformed state yields equal capacitance for both embedded sensors b) under normal load, the change for both sensors are equal since both experience equal amounts of compression c) under shear load, both sensors have completely different readings since one experiences tension while the other experiences compression [45]

3) Piezoelectric Sensors: Piezoelectric sensors, the third type, rely on the piezoelectric effect, whose working pricniple is shown in Equation 7. In this equation, Q represents the charge generated by an applied force F, and d is the charge sensitivity of the piezoelectric material, also known as the piezoelectric constant. This effect occurs due to the displacement of cations and anions or the alignment of the permanent dipole moment within the material. The piezoelectric constant quantifies the material's ability to convert mechanical loads into piezoelectric potential. Inorganic materials like PZT, ZnO, CdS, AlN, and GaN generally exhibit a high piezoelectric constant, making them sensitive to applied loads. However, their high Young's modulus restricts their use in soft tactile sensors. PVDF, in contrast, offers intrinsic flexibility but has a lower piezoelectric constant. Researchers have combined inorganic piezoelectric materials with polymer matrices to balance dielectric and mechanical properties [46]. Currently, PVDF-based sensors are the most popular choice due to their lightweight, robustness, and chemical inertness, which make them suitable for various applications. Embedding these sensors in elastomers further enhances their adaptability for specific use cases. Figure 22 presents an exploded view of a simple piezoelectric sensor [31, 36, 37, 47].

$$Q = dF \tag{7}$$

Piezoelectric sensors offer the significant advantage of not requiring a continuous power supply, making them energy-efficient and reliable. They also provide high sensitivity and strong output signals, which are particularly beneficial for applications such as spiking neural networks (SNN). Compared to capacitive sensors, piezoelectric sensors are less complex and more cost-effective, though they remain more expensive than resistive alternatives. Additionally, their lower latency enhances their suitability for real-time applications [31, 36, 47].

Despite their advantages, piezoelectric sensors are limited to dynamic applications, as they only detect transient changes in force. While they exhibit high sensitivity within a specific frequency range, their performance diminishes at low frequencies, making them unsuitable for static force measurements. These sensors also require relatively complex signal conditioning circuitry, such as a charge amplifier, which increases their overall cost. Additionally, like resistive sensors, piezoelectric sensors are sensitive to temperature variations, which can compromise their accuracy [10, 31, 36].

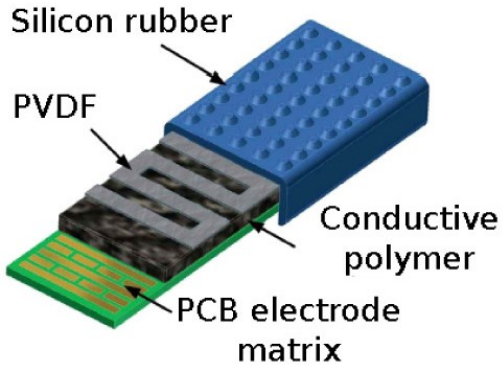

Fig. 22. Exploded view of a basic Piezoelectric sensing array with electrodes on the bottom layer, piezoelectric material in the middle and rubber on the top [48]

4) Optical Sensors: The fourth and final type of sensor discussed extensively is optical sensors, which operate based on the principles of light interaction, such as refraction, reflection, and intensity modulation, in response to external forces. They may use a number of properties of light including but not limited to phase, the propagation path, reflection, wavelength, polarization, color, and intensity. They are usually divided into index and camera-based sensors. Index-based sensors uses the properties of such as optical reflection or propagation for tactile sensing. Camera-based sensors monitors the changes in light intensity or the color of the device when interacting with the applied force via a charge coupled device (CCD) or complementary metal oxide semiconductor (CMOS) camera [46].

One common index-based sensor involves polymer optical fibers (POFs), where applied pressure causes light from the LED to scatter. The intensity of the scattered light changes proportionally to the applied pressure, enabling single-axis measurements, as illustrated in Figure 23. For greater sensitivity to shear forces, some sensors adopt a nodular fingerprint design, incorporating a dome structure that uses total internal reflection to direct light into the optofibers. This setup, shown in Figure 24, supports three-axis force measurements. The last index-based sensor system discussed uses Fiber Bragg Grating (FBG) Technology. When a load is applied, the material's refractive properties change due

to photoelasticity. By knowing the photoelastic coefficient P_e of the material, one can use Equation 8 to calculate the strain ϵ and, consequently, the force applied along a specific axis. To perform this calculation, it is necessary to first measure λ_B, the wavelength under zero load, and then measure the wavelength shift $\Delta\lambda_B$ during the load. If temperature variations ΔT occur, the calculation must also account for the material's thermal expansion coefficient α and thermo-optical coefficient ξ [10, 49–51].

$$\frac{\Delta\lambda_B}{\lambda_B} = (\alpha + \xi)\Delta T + (1 + P_e)\epsilon \tag{8}$$

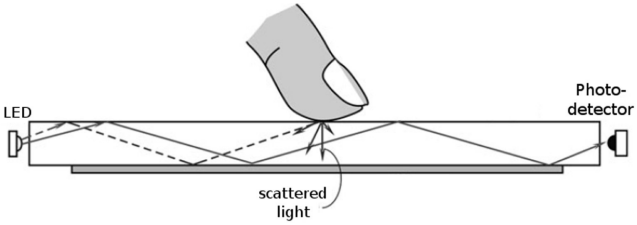

Fig. 23. Polymer Optical Fiber (POF) tactile sensor utilizing its working principle of total internal reflection, when a force is applied it "frustrates" the process and therefore the intensity of light the detector decreases[52]

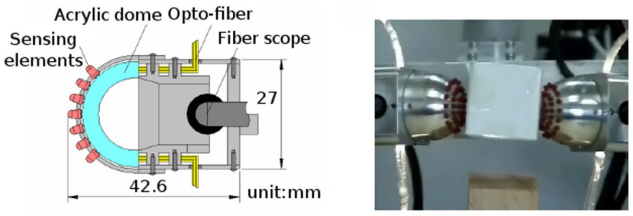

Fig. 24. 3D Optical tactile sensor configuration (left), any deformation of the sensing elements causes changes in light propogation to the opto-fibers. The sensors used as fingertips (right) for grasping and manipulating a light paper box [53]

Other prominent configuration includes camera-based systems like the TacTip line of sensors. These use an LED ring and high-resolution cameras aligned to directly capture deformation details at the sensing tip. TacTip sensors are modular, offering various designs, such as nodular fingerprints or flat tips, to suit specific applications, as demonstrated in Figure 25 [54].

The primary advantages of optical sensors include their exceptionally high spatial resolution, as individual camera pixels deliver distinct and detailed information. This allows sub-millimeter precision and enables the detection of fine surface features such as texture and roughness. Properly configured optical sensors can consistently detect slippage, making them indispensable for precision grasping tasks. Additionally, their latency can be low, depending on the computational delay, which supports real-time applications. These sensors are immune to electromagnetic interference

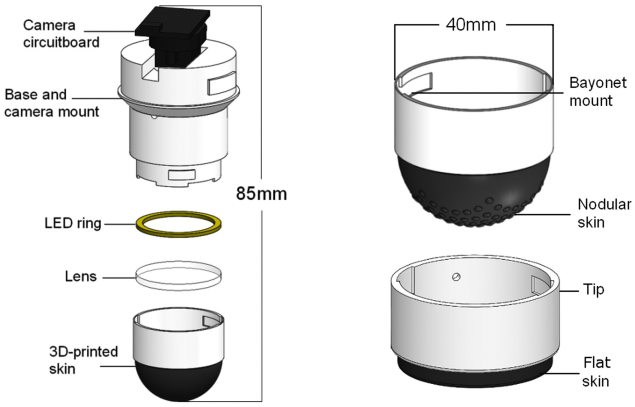

Fig. 25. Exploded View of the improved TacTip Sensor (left), the base houses a webcam which is illuminated by an led ring. The modular tips with 3D-printed rubber skin (right) can have several configurations including a nodular fingerprint (above) and flat tip (below) [55]

and remain temperature-insensitive, ensuring reliable operation across diverse environments and compatibility with various electronics [10, 31, 54].

Despite these advantages, optical sensors have notable drawbacks. They are typically bulkier than other tactile sensing technologies due to the inclusion of cameras, LEDs, and associated hardware. They also consume significantly more power, driven in part by the computational demands of processing the extensive data streams captured by cameras. Moreover, the elastomer layer used in some designs can experience hysteresis, causing performance degradation over time. Depending on the material, external lighting conditions may also impact sensor performance [10, 55].

5) Miscellaneous Sensors: Several other types of tactile sensors, while not discussed in detail, offer significant utility depending on the application.

Magnetic sensors rely on changes in magnetic flux or field intensity caused by external forces, generating voltage through the Hall effect. These sensors provide excellent sensitivity, low hysteresis, and good repeatability. However, they face challenges such as complex manufacturing processes, susceptibility to electromagnetic noise, and gradual loss of magnetization over time [36, 50, 56].

Electrical impedance tomography (EIT) exploits variations in electrical impedance distribution on a deformable object's surface under force. The system uses two electrode sets surrounding a conductive sensing area: one injects electric current, while the other measures the resulting potential distribution, which changes based on the applied force [56, 57].

Acoustic sensing transmits ultrasonic signals toward the contact surface, which reflect back to a receiver film. Surface deformations alter wave propagation, enabling tactile mapping [56, 58]. A notable example is the BioTac sensor, which combines tactile and vibration sensing. This sensor uses an incompressible liquid as an acoustic conductor to transmit

vibrations from the contact surface to a wide-bandwidth pressure transducer. However, this approach requires precise signal conditioning to suppress noise and detect subtle vibrations [59].

Biomimetic vibrissal sensors, inspired by mammalian whiskers, are lightweight and modular, making them suitable for applications like real-time contour following on drones. These whisker-based sensors use MEMS barometers across three axes to estimate contact distances and surface orientations with high accuracy [60, 61].

Several tactile sensing systems combine multiple techniques to address individual weaknesses. For instance, the GTac sensor, inspired by the multilayered mechanoreceptors in human hands, features extrinsic and intrinsic sensing layers. The extrinsic layer integrates an array of piezoresistive sensors, while the intrinsic layer employs magnetic Hall sensors. This design enables the detection of normal and shear forces with high spatial resolution. Figure 26 shows an exploded view of its layout [62]. Another biomimetic design merges EIT and acoustic sensing. In this configuration, EIT sensors detect deep pressures or deformations, while acoustic sensors capture dynamic stimuli or vibrations, resulting in a versatile tactile sensing system [63].

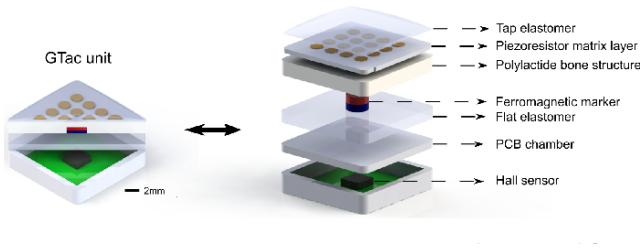

Fig. 26. Exploded View of a GTac Sensor showcasing the multilayer structure and components, the GTac sensor combines the extrinsic piezoresistor sensor with the intrinsic magnetic sensor [62]

6) Conclusion: Despite significant advancements, several challenges persist in the development and deployment of tactile sensors. These sensors often add weight and demand substantial computational resources for real-time data processing, which can strain aerial platforms with limited payload capacity and onboard processing power. Environmental factors such as temperature fluctuations, humidity, and surface contaminants further degrade sensor performance, raising reliability concerns in outdoor applications.

Addressing these limitations requires further research into tactile systems that are lightweight, highly sensitive, and energy-efficient. These systems must also demonstrate robustness against electromagnetic interference, temperature variations, and moisture exposure. Additionally, achieving minimal performance degradation over time and ensuring high repeatability remain critical goals. While some sensors meet a subset of these criteria, none currently fulfill all of them simultaneously, necessitating trade-offs based on specific application requirements [10, 36].

IV. DIGIT Sensor

The DIGIT sensor, developed by Lambeta et al., provides a compact, low-cost, and high-resolution solution for enhancing tactile perception in robotic applications. It departs from traditional tactile systems, which typically rely on resistive, capacitive, or piezoelectric sensing methods, by employing optical sensing principles. This approach enables the DIGIT sensor to capture high-resolution images of contact deformations, offering detailed tactile information such as normal and shear forces, contact geometry, and texture feedback with exceptional precision. By integrating the versatility, sensitivity, and spatial resolution of optical sensors with the affordability and compactness of resistive and capacitive technologies, the DIGIT sensor paves the way for advancements in robotic manipulation, dynamic interactions, and aerial robotics applications [11].

A. Design

The DIGIT sensor consists of a soft elastomer layer, a camera, and an integrated multicolor LED illumination system. The elastomer layer, constructed from deformable and durable materials, acts as the contact surface, where external forces induce visible deformations. Embedded LEDs provide uniform illumination for these deformations, which the onboard camera captures in real time as high-resolution images. Figure 27 illustrates the sensor's overall layout. Optical images are processed to extract critical tactile information, including force distribution, contact points, and surface patterns.

For different applications, the elastomer's properties can be tailored. A plain, reflective elastomer enhances deformation visibility, while versions embedded with markers support optic flow methods for more detailed analysis. Alternatively, a transparent elastomer is used when external visibility is crucial. Figure 28 demonstrates how changes in elastomer properties influence the sensor's functionality [11].

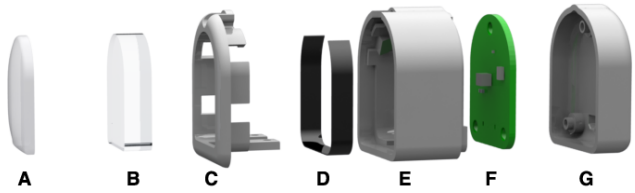

Fig. 27. Exploded view of a DIGIT sensor. A) elastomer, B) acrylic window, C) snap-fit holder, D) lighting PCB, E) plastic housing, F) camera PCB, G) back housing [11]

The DIGIT sensor differentiates itself from other tactile systems in several critical aspects. Unlike capacitive and resistive sensors, which rely on electrical conductivity and often face challenges with irregular surfaces or non-conductive materials, the DIGIT sensor leverages optical

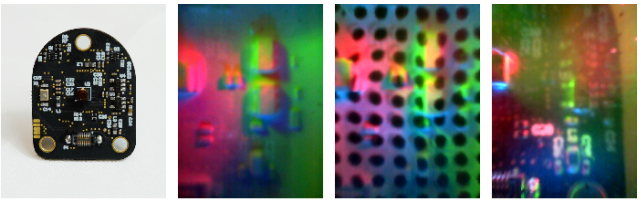

Fig. 28. Effect of different types of elastomers on a DIGIT sensor, the three different types chosen here (left to right) are reflective, reflective with markers and transparent [11]

methods to ensure reliable performance across diverse material types. Its sub-millimeter precision captures intricate surface deformations, significantly surpassing the resolution of conventional tactile sensors. Figure 29 provides examples of the detailed information the DIGIT sensor can extract.

Additionally, its modular and lightweight design facilitates straightforward integration into robotic platforms, such as end-effectors or grippers, without necessitating substantial structural modifications. While bulkier systems like the TacTip sensor offer comparable functionality, the DIGIT sensor's compact form factor enhances its adaptability. However, its size remains a constraint for applications with severe spatial limitations, such as aerial robotics [11].

One of the most significant advantages of the DIGIT sensor is its support for real-time tactile feedback. Operating at frame rates of up to 60 frames per second, the sensor processes tactile data dynamically, enabling responsive manipulation tasks. This capability is especially valuable in robotic applications where fine adjustments are crucial. For instance, during object grasping and manipulation, the sensor detects subtle changes in force imbalances and surface deformations, allowing the robotic system to adjust its grip in real time. This prevents slippage and excessive force. Lambeta et al. showcased this ability by integrating the DIGIT sensor into a robotic hand, where it manipulated small objects, such as marbles, with remarkable precision and control, as shown in Figure 30. Such capabilities position the DIGIT sensor as a transformative tool for robotic manipulation, particularly in tasks demanding both dexterity and sensitivity [11].

The DIGIT sensor's performance relies on an initial calibration process to ensure consistent and accurate results. During calibration, relationships between observed elastomer deformations and corresponding applied forces are established, often through controlled experiments with known forces and contact geometries. This step is essential for translating raw optical images into meaningful tactile information and minimizing errors caused by sensor variability [11].

Additionally, the high-resolution tactile images captured by the DIGIT sensor require advanced data processing techniques to extract useful information, such as force distribution and contact patterns. Modern machine learning methods, particularly Convolutional Neural Networks (CNNs), play a crucial role in this process. CNNs identify intricate deformation features and correlate them to specific physical properties, such as pressure magnitude and direction. These algorithms enhance the sensor's ability to detect subtle changes, such as shear forces or slip events, which are critical for tasks like object manipulation. By incorporating machine learning, the DIGIT sensor achieves reliable and efficient data interpretation [11].

The DIGIT sensor's high-resolution tactile feedback also enables applications in texture recognition and surface mapping. By analyzing the deformation patterns produced upon contact, the sensor distinguishes between materials of varying stiffness, textures, and geometries. This capability has significant implications for tasks such as material sorting in manufacturing environments, quality control in industrial processes, and tactile exploration in unknown environments. The sensor's ability to detect subtle surface variations further enhances its potential for precision tasks that require detailed tactile information, such as inspecting fragile or irregularly shaped objects [11].

Despite its many strengths, the DIGIT sensor is not without limitations. Its reliance on optical sensing principles makes it vulnerable to environmental factors such as lighting variability, temperature fluctuations, and contamination of the elastomer surface. External light sources or dirt can interfere with image quality, potentially degrading performance in uncontrolled or outdoor settings. Additionally, processing high-resolution tactile images imposes significant computational demands, particularly for real-time applications. This requirement may strain robotic platforms with limited onboard processing capabilities, such as drones or lightweight autonomous systems.

While the elastomer layer is designed to withstand repeated use, it remains subject to wear and tear over time, posing challenges for long-term durability, especially in harsh or high-stress environments. However, this is somewhat mitigated by the modular design, as the elastomer layer can be replaced independently of the rest of the sensor. Compared to simpler tactile systems, the DIGIT sensor's current form factor, though compact, may still be considered bulky for ultra-constrained platforms like small drones.

Nevertheless, the DIGIT sensor's modular construction and low manufacturing cost make it a highly accessible and scalable solution for both research and industry. Its design democratizes access to advanced tactile sensing technologies, which have historically been expensive or difficult to implement. Looking forward, improvements in elastomer materials would enhance the sensor's durability and resilience to environmental contaminants as well as reduce hysteresis upon repeated load cycles, while advancements in processing algorithms would reduce computational overhead. Additionally, integrating the DIGIT sensor with other sensing modalities—such as temperature, vibration, or magnetic sensing—would create multi-modal tactile systems capable of delivering even richer feedback. Such developments would further expand the sensor's utility across diverse applications, including robotic manipulation, aerial robotics, and human-robot interaction

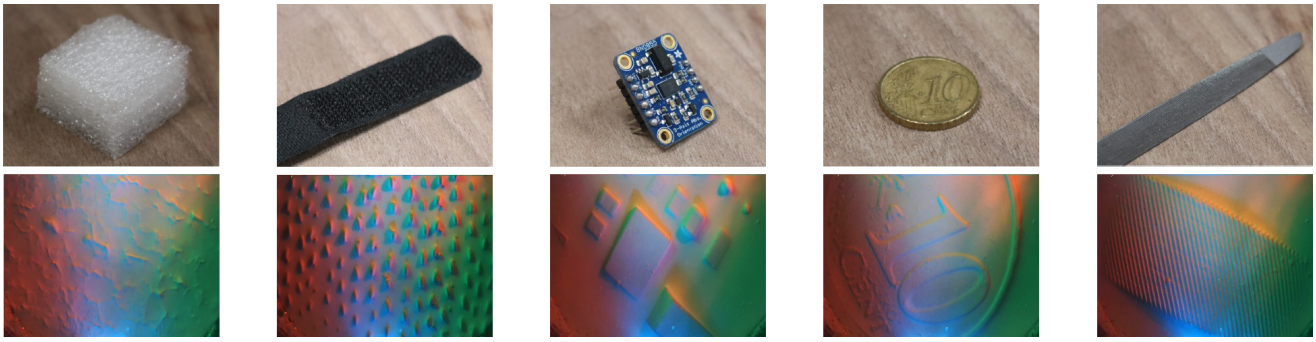

Fig. 29. Object under test and corresponding raw measurements taken using DIGIT, the sensor is able to capture sub-millimeter details which gives detailed information information about the texture of the test surface, this also highlights the advantage of a multicolored led array as small details are more pronounced [12]

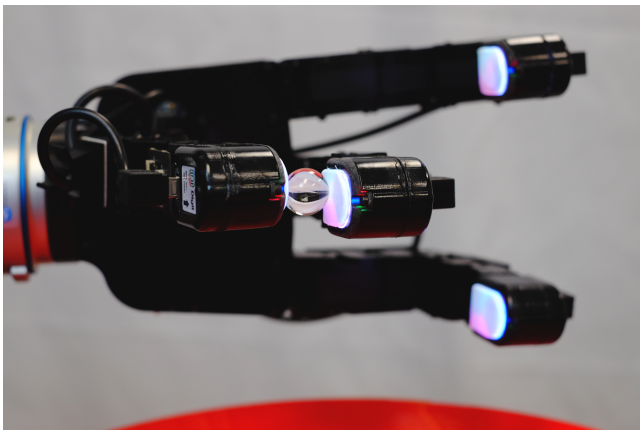

Fig. 30. Marble manipulation using DIGIT sensors mounted on an Allegro multi-finger hand. The robotic hand pinches the marble between its thumb and another finger and rolls it over its finger to manipulate it to the desired location [11]

B. Applications

Since the DIGIT sensor is a recent innovation, there have not been many research papers exploring its use in various applications. However, a few notable examples demonstrate its capabilities. One such example is the DigiTac sensor, a hybrid system that combines the strengths of both the DIGIT and TacTip sensors. DigiTac utilizes the DIGIT's base design, including its lighting, camera board, and housing, while integrating the TacTip's nodular fingerprint sensing module, which features a 3D-printed skin/mount, window, and soft gel. The adapted TacTip module is illustrated in Figure 31. The motivation behind this hybrid design is to compare the relatively flat and inelastic sensing surface of the DIGIT sensor to the soft, curved sensing surface of the TacTip. A visual comparison of the outputs produced by all three sensors is provided in Figure 32 [64].

In experiments focused on pose prediction and pose-based tactile servo control, all three sensors demonstrated satisfactory performance. However, the design of the DIGIT housing introduced biasing of the contact angle during servo control tasks. This issue arose because the DIGIT's stiff and relatively non-compliant design was less capable of adapting to asymmetrical loading. For the edge-following task, all three sensors performed well. However, the DIGIT sensor struggled in the surface-following task due to its flat and stiff elastomer layer, which was not well-suited for sliding smoothly over surfaces. During the experiments, which included thousands of sliding contact cycles to train and test their models, the team encountered durability issues. Specifically, one DigiTac sensor failed when the skin tore at the junction with its housing, and one DIGIT sensor was damaged when its elastomer layer sheared off following a collision with the test object [64].

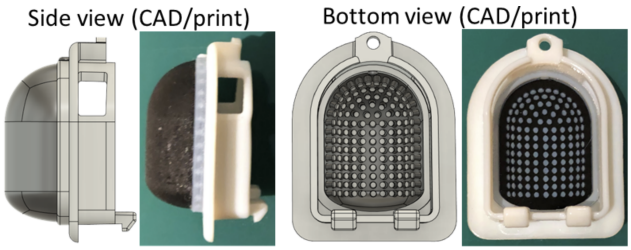

Fig. 31. The 3-D printed DigiTac sensing module utilizing a press-fit housing which can be used to attach it to the normal DIGIT base, it offers the compact design of the DIGIT while offering a curved, elastic sensing surface[64]

Another application utilizes DIGIT sensors to manipulate objects while simultaneously performing Simultaneous Localization and Mapping (SLAM). This allows the system to map the entire model of an object autonomously without needing to move its base. The object reconstruction was found to be highly precise, achieving F-scores of 81% with pose drifts of just 4.7 mm, which were further reduced to 2.3 mm when using known CAD models. Additionally, the approach significantly outperformed vision-based methods under heavy occlusion, demonstrating up to a 94% improvement in pose tracking. The setup involving ground-based robots used for the experiments, along with the correspond-

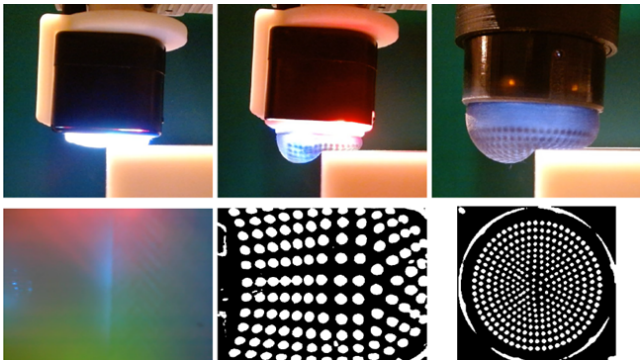

Fig. 32. DIGIT, DigiTac and TacTip sensor readings when pressed against an edge, all three are able to detect it clearly. The normal DIGIT sensor (left) shows a color shift at the edge, the DigiTac (middle) and TacTip (right) show a shift in the pattern to signify an edge [64]

ing reconstructions, is shown in Figure 33 [65].

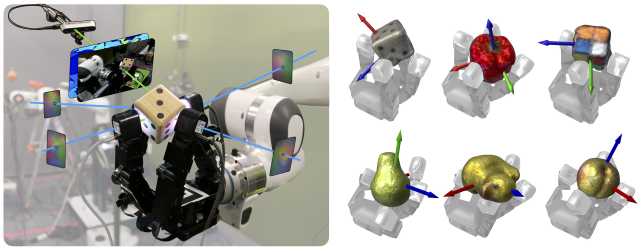

Fig. 33. 3D reconstruction of an object using a DIGIT SLAM implementation, it estimates the pose and shape of objects from a stream of visual, tactile and proprioceptive data [65]

V. Challenges and Opportunities

Through an analysis of the existing research in this field, it becomes evident that while significant progress has been made in developing grasping drones, perching drones remain a relatively new and underexplored area. Furthermore, the perching drones that do exist tend to be rudimentary, lacking closed-loop feedback systems. Another limitation is that nearly all perching drones with grippers or claws position these mechanisms at the bottom of the drone. This design choice necessitates large landing skids or other creative solutions to ensure the drone can land on the ground.

Mounting the perching mechanism at the top of the drone eliminates interference with landing, thereby reducing the need for additional structural components. This, in turn, saves weight, improves flight efficiency, and simplifies the task of the perching mechanism. Additionally, a top-mounted perching system is likely to achieve a more stable passive perch, making it more robust against external disturbances such as wind. This presents a significant opportunity to explore a unique design with clear advantages over conventional approaches.

Similarly, the DIGIT sensor remains largely under-investigated, with minimal research exploring its applications, particularly in aerial manipulators. From the studies conducted so far, it is evident that the DIGIT sensor requires a Convolutional Neural Network (CNN) to be trained for calibration. However, once calibrated, the sensor has shown strong performance in pose estimation and pose-based tactile servo control. These findings are encouraging for its use in a perching application.

At present, most aerial manipulators do not integrate tactile sensing into their control systems. Applying tactile data—similar to its use in ground-based robotics—represents an excellent opportunity for innovation. However, the DIGIT sensor is relatively bulky, which poses a challenge for aerial applications. To compensate for its weight, the rest of the drone design must be extremely lightweight. The current plan involves using four DIGIT sensors to maximize the tactile sensing domain, with one sensor placed at each of the three fingertips and one at the base of the gripper.

While full force or pose-based servo control may not be achievable, the integration of pose and force estimation will still provide significant information about the bar's position relative to the drone and the security of the grasp before shutting down the motors. Therefore, the control strategy will likely be relatively simple, with the tactile sensors not directly serving as closed-loop controllers but still offering highly valuable feedback to the system.

If this drone successfully integrates tactile sensing for secure and autonomous perching from any orientation, it will represent a major advancement in aerial robotics. This innovation will help bridge the gap between aerial and ground-based robotics in terms of robustness and utility. Such a system will have a wide range of applications, from energy-saving perching for environmental surveying to applications in precision agriculture.

VI. Conclusion

This literature study explores the advancements and challenges associated with tactile sensing and perching mechanisms, particularly in the context of aerial robotics. The analysis covers a wide range of topics, including the evolution of aerial manipulator and gripper designs, the limitations of vision-based and radar-based systems, different tactile sensing technologies and the role of tactile feedback in enabling robust interaction with the environment. It aims to build upon a previous design of a perching drone which utilized an underactuated compliant mechanism with capacitive tactile sensors. It emphasizes the usage of higher resolution DIGIT sensors, providing information on their capabilities, shortcomings, and potential applications in aerial perching tasks.

The review identifies a significant gap in the integration of tactile sensing within aerial robotics, a domain still heavily reliant on vision-based systems despite their inherent limitations in occluded and low-light scenarios. While ground-based robotics have made substantial progress in leveraging tactile feedback for manipulation tasks, aerial systems remain in the nascent stages of adopting such technologies. The DIGIT sensor, despite its bulk, weight and rigid design when

compared to other sensing technologies, shows promise in providing accurate pose and force estimation when combined with machine learning algorithms. This will further aid in adding functionality to the perching drone.

In the context of perching mechanisms, the study highlights the predominance of bottom-mounted grippers and their associated trade-offs, such as added weight and compromised landing stability. Novel approaches, such as mounting grippers on top of drones, are proposed as promising alternatives that could enhance stability, reduce energy consumption, and enable more efficient perching in varied environments. It also notes that for the few perching mechanisms that have been designed, none of them integrate tactile sensing and rather rely on an open-loop control system which is not very robust or effective.

This comprehensive analysis underscores several opportunities for future research. First, integrating tactile feedback into aerial robotic systems offers the potential to bridge the gap between aerial and ground-based robotics in terms of control and robustness. Second, lightweight, modular designs are crucial for compensating for the added weight of higher resolution sensors. Finally, the study advocates for exploring the synergy between vision and tactile sensing to create robust multimodal systems capable of addressing the complex challenges of aerial manipulation.

Research Question

The resulting primary research question from this literature study is: **How can the integration of high-resolution tactile sensors enhance the functionality, adaptability, and robustness of a perching drone, enabling it to autonomously perch regardless of its initial position and orientation?**

- Sensor Integration and Capabilities
  - What are the limitations of the previous tactile sensing system, and how do higher resolution sensors address these shortcomings?
  - How can the chosen high-resolution sensors be integrated into the drone's gripper design while maintaining inherent compliance and lightweight properties?
  - What type of data can the sensors provide, and how can this data be processed to inform the perching maneuver?
- Performance Evaluation
  - How does the performance of the perching drone with the new sensors compare to the previous iteration in terms of accuracy, reliability, and adaptability?
  - What metrics can be used to evaluate the drone's performance?
- Design and Weight Optimization
  - How can the drone's design, including the gripper and tactile sensor placement, be optimized for weight reduction while maintaining functionality?
  - What materials and manufacturing techniques can be employed to ensure the drone is lightweight and efficient for perching tasks?
- Broader Applications and Scalability
  - Beyond bar perching, how can the drone's enhanced tactile sensing capabilities be leveraged for other applications?
  - What are the potential limitations or constraints of using the chosen sensors in real-world scenarios, such as environmental conditions or payload restrictions?
  - How can the system be scaled or adapted for more complex tasks, such as perching on non-cylindrical or moving objects?

References

[1] Chenghai Zhang and John M. Kovacs. "The application of small unmanned aerial systems for precision agriculture: A review". In: *Precision Agriculture* 13.6 (2012), pp. 693–712.

[2] Francesco Nex and Fabio Remondino. "UAV for 3D mapping applications: A review". In: *Applied Geomatics* 6 (2014), pp. 1–15.

[3] Fabio Ruggiero, Vincenzo Lippiello, and Anibal Ollero. "Aerial manipulation: A literature review". In: *IEEE Robotics and Automation Letters* 3.3 (2018), pp. 1957–1964.

[4] Jiawei Meng et al. "On aerial robots with grasping and perching capabilities: A comprehensive review". In: *Frontiers in Robotics and AI* 8 (2022).

[5] Wenzhen Yuan, Siyuan Dong, and Edward H. Adelson. "Gelsight: High-resolution robot tactile sensors for estimating geometry and force". In: *Sensors* 17.12 (2017), p. 2762.

[6] Karen Bodie et al. "An Omnidirectional Aerial Manipulation Platform for Contact-Based Inspection". In: *CoRR* abs/1905.03502 (2019). URL: https://arxiv.org/abs/1905.03502.

[7] Salua Hamaza, Ioannis Georgilas, and Thomas Richardson. "2D Contour Following with an Unmanned Aerial Manipulator: Towards Tactile-Based Aerial Navigation". In: *2019 IEEE/RSJ International Conference on Intelligent Robots and Systems (IROS)*. IEEE, 2019, pp. 3664–3669.

[8] Luqiang Zheng and Salua Hamaza. "ALBERO: Dynamic Aerial Landing on Branches for Environmental Robotics Operations". In: *IEEE Robotics and Automation Letters* (2023).

[9] Anish Vidurprakash Jadoenathmisier. "Aerial Perching via Active Touch: Embodying Robust Tactile Grasping on Aerial Robots". In: *MSc Thesis, Delft University of Technology* (Dec. 2023). Available at: http://resolver.tudelft.nl/uuid:f7ec9e1c-15db-4982-b2fa-4ba0f51a5b91.

[10] Zhanat Kappassov, Juan-Antonio Corrales, and Véronique Perdereau. "Tactile sensing in dexterous robot hands—Review". In: *Robotics and Autonomous Systems* 74 (2015), pp. 195–220.

[11] Michael Lambeta et al. “DIGIT: A novel design for a low-cost compact high-resolution tactile sensor”. In: *Conference on Robot Learning*. 2020, pp. 1–10.

[12] Inc. GelSight. *DIGIT Tactile Sensor*. https://www.gelsight.com/product/digit-tactile-sensor/. Accessed: 2024-11-24.

[13] Alejandro Lopez-Lora et al. “MHYRO: Modular HYbrid RObot for contact inspection and maintenance in oil & gas plants”. In: *2020 IEEE/RSJ International Conference on Intelligent Robots and Systems (IROS)*. Las Vegas, NV, USA: IEEE, 2020, pp. 1268–1275. DOI: 10.1109/IROS45743.2020.9341639.

[14] Pablo Ramon Soria, Begoña C. Arrue, and Anibal Ollero. “Detection, Location and Grasping Objects Using a Stereo Sensor on UAV in Outdoor Environments”. In: *Sensors* 17.1 (2017). ISSN: 1424-8220. DOI: 10.3390/s17010103. URL: https://www.mdpi.com/1424-8220/17/1/103.

[15] Ziyu Chen et al. “A Review of Soft Manipulators for Applications in Aerial Robotics”. In: *Soft Robotics* 8.6 (2021), pp. 776–798.

[16] Daniela Rus and Michael T. Tolley. “Design, Fabrication, and Control of Soft Robots”. In: *Nature* 521 (2015), pp. 467–475.

[17] Alejandro Suarez et al. “Aerial physical interaction in grabbing conditions with lightweight and compliant dual arms”. In: *Applied Sciences* 10.24 (2020), p. 8927.

[18] Dominik Müller, Joachim Grasmeyer, and Ryan Bertrand. “Perching and resting–A paradigm for UAV maneuvering with modularized landing gears”. In: *AIAA Guidance, Navigation, and Control Conference*. AIAA, 2011, pp. 1234–1243.

[19] K. Zhang et al. “SpiderMAV: Perching and stabilizing micro aerial vehicles with bio-inspired tensile anchoring systems”. In: *2017 IEEE/RSJ International Conference on Intelligent Robots and Systems (IROS)*. Vancouver, BC, Canada: IEEE, 2017, pp. 6849–6854. DOI: 10.1109/IROS.2017.8206606.

[20] Amir Kalantari et al. “Autonomous perching and takeoff on vertical walls for a quadrotor micro air vehicle”. In: *2015 IEEE International Conference on Robotics and Automation (ICRA)*. IEEE. 2015, pp. 4669–4674.

[21] Elliot W Hawkes, Hao Jiang, and Mark R Cutkosky. “Three-dimensional dynamic surface grasping with dry adhesion”. In: *The International Journal of Robotics Research* 35.8 (2016), pp. 943–958.

[22] Alain Lussier Desbiens, Alan T Asbeck, and Mark R Cutkosky. “Landing, perching and taking off from vertical surfaces”. In: *The International Journal of Robotics Research* 30.3 (2011), pp. 355–370.

[23] Xinyu Guo et al. “Powerful UAV manipulation via bioinspired self-adaptive soft self-contained gripper”. In: *Science Advances* 10 (2024), eadn6642. DOI: 10.1126/sciadv.adn6642.

[24] Raymond R. Ma, Lael Odhner, and Aaron M. Dollar. “A modular, open-source 3D printed underactuated hand”. In: *2013 IEEE International Conference on Robotics and Automation* (2013), pp. 2737–2743. URL: https://api.semanticscholar.org/CorpusID:18511615.

[25] Aaron M. Dollar and Robert D. Howe. “The Highly Adaptive SDM Hand: Design and Performance Evaluation”. In: *The International Journal of Robotics Research* 29.5 (2010), pp. 585–597. DOI: 10.1177/0278364909360852.

[26] Spencer B. Backus, Lael U. Odhner, and Aaron M. Dollar. “Design of hands for aerial manipulation: Actuator number and routing for grasping and perching”. In: *2014 IEEE/RSJ International Conference on Intelligent Robots and Systems*. 2014, pp. 34–40. DOI: 10.1109/IROS.2014.6942537.

[27] Pauline Pounds and Aaron Dollar. “Hovering Stability of Helicopters With Elastic Constraints”. In: Jan. 2010. DOI: 10.1115/DSCC2010-4166.

[28] Spencer B. Backus and Aaron M. Dollar. “Design Optimization of a Prismatic-Revolute-Revolute Joint Hand for Grasping From Unconstrained Vehicles”. In: 2017. URL: https://api.semanticscholar.org/CorpusID:49673842.

[29] Courtney E Doyle et al. “An avian-inspired passive mechanism for quadrotor perching”. In: *IEEE/ASME Transactions On Mechatronics* 18.2 (2012), pp. 506–517.

[30] Haruhisa Kawasaki, Takeshi Komatsu, and Kanji Uchiyama. “Dexterous anthropomorphic robot hand with distributed tactile sensor: Gifu hand II”. In: *IEEE/ASME Transactions on Mechatronics* 7.3 (2002), pp. 296–303. DOI: 10.1109/TMECH.2002.802720.

[31] Hanna Yousef, Mehdi Boukallel, and Kaspar Althoefer. “Tactile sensing for dexterous in-hand manipulation in robotics—A review”. In: *Sensors and Actuators A: Physical* 167.2 (2011). Solid-State Sensors, Actuators and Microsystems Workshop, pp. 171–187. ISSN: 0924-4247. DOI: https://doi.org/10.1016/j.sna.2011.02.038. URL: https://www.sciencedirect.com/science/article/pii/S0924424711001105.

[32] Chen Xu et al. “Three-dimensional micro strain gauges as flexible, modular tactile sensors for versatile integration with micro- and macroelectronics”. In: *Science Advances* 10.34 (2024), eadp6094. DOI: 10.1126/sciadv.adp6094. URL: https://www.science.org/doi/abs/10.1126/sciadv.adp6094.

[33] Stefano Stassi et al. “Flexible Tactile Sensing Based on Piezoresistive Composites: A Review”. In: *Sensors* 14.3 (2014), pp. 5296–5332. ISSN: 1424-8220. URL: https://www.mdpi.com/1424-8220/14/3/5296.

[34] Karsten Weiss and Heinz Wörn. “The working principle of resistive tactile sensor cells”. In: *IEEE International Conference Mechatronics and Automation,*

2005 1 (2005), 471–476 Vol. 1. URL: https://api.semanticscholar.org/CorpusID:38435560.

[35] Haokun Yi et al. "Conductive polymer composites for resistive flexible strain sensors". In: *Polymer* 307 (2024), p. 127286. ISSN: 0032-3861. DOI: https://doi.org/10.1016/j.polymer.2024.127286. URL: https://www.sciencedirect.com/science/article/pii/S0032386124006220.

[36] Mahmoud Meribout et al. "Tactile sensors: A review". In: *Measurement* 238 (2024), p. 115332. ISSN: 0263-2241. DOI: https://doi.org/10.1016/j.measurement.2024.115332. URL: https://www.sciencedirect.com/science/article/pii/S026322412401217X.

[37] J. Xi et al. "Recent Advances in Tactile Sensory Systems: Mechanisms, Fabrication, and Applications". In: *Nanomaterials (Basel)* 14.5 (Mar. 2024), p. 465. DOI: 10.3390/nano14050465.

[38] Bing Zhu et al. "Highly Stretchable and Sensitive Multimodal Tactile Sensor Based on Conductive Rubber Composites to Monitor Pressure and Temperature". In: *Polymers* 14 (2022). URL: https://api.semanticscholar.org/CorpusID:247687149.

[39] Hassan Alirezaei, Akihiko Nagakubo, and Yasuo Kuniyoshi. "A highly stretchable tactile distribution sensor for smooth surfaced humanoids". In: *2007 7th IEEE-RAS International Conference on Humanoid Robots*. 2007, pp. 167–173. DOI: 10.1109/ICHR.2007.4813864.

[40] H.B. Muhammad et al. "Development of a bioinspired MEMS based capacitive tactile sensor for a robotic finger". In: *Sensors and Actuators A: Physical* 165.2 (2011), pp. 221–229. ISSN: 0924-4247. DOI: https://doi.org/10.1016/j.sna.2010.10.025. URL: https://www.sciencedirect.com/science/article/pii/S0924424710004838.

[41] Hong-Ki Kim, Seunggun Lee, and Kwang-Seok Yun. "Capacitive tactile sensor array for touch screen application". In: *Sensors and Actuators A: Physical* 165.1 (2011). Transducers 2009, pp. 2–7. ISSN: 0924-4247. DOI: https://doi.org/10.1016/j.sna.2009.12.031. URL: https://www.sciencedirect.com/science/article/pii/S0924424709005573.

[42] Sheng Li et al. "Bimodal capacitive tactile sensor assisted by shield effect of triboelectric nanogenerator". In: *Nano Energy* 118 (2023), p. 108946. ISSN: 2211-2855. DOI: https://doi.org/10.1016/j.nanoen.2023.108946. URL: https://www.sciencedirect.com/science/article/pii/S2211285523007838.

[43] Haicheng Gu et al. "A Battery-Free Wireless Tactile Sensor for Multimodal Force Perception". In: *Advanced Functional Materials* n/a.n/a (), p. 2410661. DOI: https://doi.org/10.1002/adfm.202410661. eprint: https://onlinelibrary.wiley.com/doi/pdf/10.1002/adfm.202410661. URL: https://onlinelibrary.wiley.com/doi/abs/10.1002/adfm.202410661.

[44] Perla Maiolino et al. "A Flexible and Robust Large Scale Capacitive Tactile System for Robots". In: *IEEE Sensors Journal* 13.10 (2013), pp. 3910–3917. DOI: 10.1109/JSEN.2013.2258149.

[45] Hyung-Kew Lee et al. "Normal and shear force measurement using a flexible polymer tactile sensor with embedded multiple capacitors". In: *Journal of Microelectromechanical Systems* 17.4 (2008), pp. 934–942.

[46] Chunfeng Wang et al. "Tactile Sensors for Advanced Intelligent Systems". In: *Advanced Intelligent Systems* 1.8 (2019), p. 1900090. DOI: https://doi.org/10.1002/aisy.201900090. URL: https://onlinelibrary.wiley.com/doi/abs/10.1002/aisy.201900090.

[47] FangXi Qi et al. "PVDF-Based Flexible Piezoelectric Tactile Sensors: Review". In: *Crystal Research and Technology* 58 (Sept. 2023). DOI: 10.1002/crat.202300119.

[48] Dirk Goger, Nicolas Gorges, and Heinz Worn. "Tactile sensing for an anthropomorphic robotic hand: Hardware and signal processing". In: *2009 IEEE International Conference on Robotics and Automation*. 2009, pp. 895–901. DOI: 10.1109/ROBOT.2009.5152650.

[49] Ni Yao and Shipeng Wang. "Recent progress of optical tactile sensors: A review". In: *Optics & Laser Technology* 176 (2024), p. 111040. ISSN: 0030-3992. DOI: https://doi.org/10.1016/j.optlastec.2024.111040. URL: https://www.sciencedirect.com/science/article/pii/S0030399224004985.

[50] Cheng Chi et al. "Recent Progress in Technologies for Tactile Sensors". In: *Sensors (Basel, Switzerland)* 18 (2018). URL: https://api.semanticscholar.org/CorpusID:4226575.

[51] Kezhen Jin et al. "Fiber Bragg grating-based fingertip tactile sensors for normal/shear forces and temperature detection". In: *Sensors and Actuators A: Physical* 357 (2023), p. 114368. ISSN: 0924-4247. DOI: https://doi.org/10.1016/j.sna.2023.114368. URL: https://www.sciencedirect.com/science/article/pii/S0924424723002170.

[52] Jacob Fraden. *Handbook of Modern Sensors: Physics, Designs, and Applications*. Springer, 2004.

[53] Hanafiah Yussof et al. "Tactile sensing-based control system for dexterous robot manipulation". In: *Advances in Computational Algorithms and Data Analysis* (2009), pp. 199–213.

[54] Nathan F. Lepora. "Soft Biomimetic Optical Tactile Sensing With the TacTip: A Review". In: *IEEE Sensors Journal* 21.19 (2021), pp. 21131–21143. DOI: 10.1109/JSEN.2021.3100645.

[55] Benjamin Ward-Cherrier et al. "The TacTip Family: Soft Optical Tactile Sensors with 3D-Printed Biomimetic Morphologies". In: *Soft Robotics* 5.2 (2018). PMID: 29297773, pp. 216–227. DOI: 10.1089/soro.2017.0052. URL: https://doi.org/10.1089/soro.2017.0052.

[56] Willow Mandil et al. "Tactile-Sensing Technologies: Trends, Challenges and Outlook in Agri-Food Manipulation". In: *Sensors (Basel, Switzerland)* 23 (2023). URL: https://api.semanticscholar.org/CorpusID:261189098.

[57] Haibin Wu et al. "New Flexible Tactile Sensor Based on Electrical Impedance Tomography". In: *Micromachines* 13.2 (2022). ISSN: 2072-666X. DOI: 10.3390/mi13020185. URL: https://www.mdpi.com/2072-666X/13/2/185.

[58] Cheng-Hsin Chuang et al. "Ultrasonic tactile sensor integrated with TFT array for force feedback and shape recognition". In: *Sensors and Actuators A-physical* 271 (2018), pp. 348–355. URL: https://api.semanticscholar.org/CorpusID:115437214.

[59] Jeremy A. Fishel and Gerald E. Loeb. "Sensing tactile microvibrations with the BioTac — Comparison with human sensitivity". In: *2012 4th IEEE RAS & EMBS International Conference on Biomedical Robotics and Biomechatronics (BioRob)*. 2012, pp. 1122–1127. DOI: 10.1109/BioRob.2012.6290741.

[60] Mahima Yoganarasimhan. "Drones' Tactile Navigation using Biomimetic Vibrissal Sensors". In: *MSc Thesis, Delft University of Technology* (2024). Available at: https://repository.tudelft.nl/record/uuid:411c4c11-8401-48e1-8977-4051d81c27f9.

[61] Martin J. Pearson et al. "Biomimetic vibrissal sensing for robots". In: *Philosophical Transactions of the Royal Society B: Biological Sciences* 366.1581 (2011), pp. 3085–3096. DOI: 10.1098/rstb.2011.0164.

[62] Zeyu Lu, Xingyu Gao, and Haoyong Yu. "GTac: A Biomimetic Tactile Sensor With Skin-Like Heterogeneous Force Feedback for Robots". In: *IEEE Sensors Journal* 22 (2022), pp. 14491–14500. URL: https://api.semanticscholar.org/CorpusID:246411150.

[63] K Park et al. "A biomimetic elastomeric robot skin using electrical impedance and acoustic tomography for tactile sensing". In: *Science Robotics* 7 (2022). URL: https://api.semanticscholar.org/CorpusID:249520303.

[64] Nathan F. Lepora et al. "DigiTac: A DIGIT-TacTip Hybrid Tactile Sensor for Comparing Low-Cost High-Resolution Robot Touch". In: *IEEE Robotics and Automation Letters* (2022). DOI: 10.1109/LRA.2022.3190641.

[65] Sudharshan Suresh et al. *Neural feels with neural fields: Visuo-tactile perception for in-hand manipulation*. 2023. arXiv: 2312.13469 [cs.RO]. URL: https://arxiv.org/abs/2312.13469.